New insights on Chlm function in Photosystem II from site-directed mutants of D1/T179 in Thermosynechococcus elongatus

Yuki Takegawa, Makoto Nakamura, Shin Nakamura, Takumi Noguchi, Julien Selles, A. William Rutherford, Alain Boussac, Miwa Sugiura

New insights on Chl_{D1} function in Photosystem II from site-directed mutants of D1/T179 in *Thermosynechococcus elongatus.*

Yuki Takegawa*[a], Makoto Nakamura*[a], Shin Nakamura[b], Takumi Noguchi[b], Julien Sellés[c], A. William Rutherford[d], Alain Boussac[e§], Miwa Sugiura[a,f§]

*These authors equally contributed to this work.

[§]Corresponding authors: miwa.sugiura@ehime-u.ac.jp, alain.boussac@cea.fr

[a]Graduate School of Science and Technology, Ehime University, Bunkyo-cho, Matsuyama, Ehime 790-8577, Japan.

[b]Division of Material Science, Graduate School of Science, Nagoya University, Furo-cho, Chikusa-ku, Nagoya, 464-8602, Japan

[c]Institut de Biologie Physico-Chimique, UMR CNRS 7141 and Sorbonne Université, 13 rue Pierre et Marie Curie, 75005 Paris, France.

[d]Department of Life Sciences, Imperial College, London SW7 2AZ, United Kingdom.

[e]I^2BC, UMR CNRS 9198, CEA Saclay, 91191 Gif-sur -Yvette, France.

[f]Proteo-Science Research Center, Ehime University, Bunkyo-cho, Matsuyama, Ehime 790-8577, Japan.

Keywords: Photosystem II; Reaction center; Chl_{D1}; P_{680}; electrochromic shifts.

Abbreviations

Chl, chlorophyll; Chl_{D1}/Chl_{D2}, monomeric Chl on the D1 or D2 side, respectively; DCMU, 3-(3,4-dichlorophenyl)-1,1-dimethylurea; DMSO, dimethyl sulfoxide; EPR, Electron Paramagnetic Resonance; FCCP, *p*-(trifluoromethoxy)-phenylhydrazone; FTIR, Fourier transform infrared; MES, 2-(*N*-morpholino) ethanesulfonic acid; P_{680}, primary electron donor; P_{D1} and P_{D2}, individual Chl on the D1 or D2 side, respectively, which constitute a pair of Chl with partially overlapping aromatic rings; $Pheo_{D1}$ and $Pheo_{D2}$, pheophytin on the D1 or D2 side, respectively; PPBQ, phenyl *p*–benzoquinone; PSII, Photosystem II; Q_A, primary quinone acceptor; Q_B, secondary quinone acceptor; TL, thermoluminescence; WT*3, *T. elongatus* mutant strain containing only the *psbA*$_3$ gene, 43-H, *T. elongatus* mutant strain which has a His-tag on C-terminus of CP43.

Abstract

The monomeric chlorophyll, Chl_{D1}, which is located between the $P_{D1}P_{D2}$ chlorophyll pair and the pheophytin, $Pheo_{D1,}$ is the longest wavelength chlorophyll in the heart of Photosystem II and is thought to be the primary electron donor. Its central Mg^{2+} is liganded to a water molecule that is H-bonded to D1/T179. Here, two site-directed mutants, D1/T179H and D1/T179V, were made in the thermophilic cyanobacterium, *Thermosynechococcus elongatus*, and characterized by a range of biophysical techniques. The Mn_4CaO_5 cluster in the water-splitting site is fully active in both mutants. Changes in thermoluminescence indicate that *i*) radiative recombination occurs *via* the repopulation of $*Chl_{D1}$ itself; *ii*) non-radiative charge recombination reactions appeared to be faster in the T179H-PSII; and *iii*) the properties of $P_{D1}P_{D2}$ were unaffected by this mutation, and consequently iv) the immediate precursor state of the radiative excited state is the $Chl_{D1}^{+}Pheo_{D1}^{-}$ radical pair. Chlorophyll bleaching due to high intensity illumination correlated with the amount of $^1O_2$ generated. Comparison of the bleaching spectra with the electrochromic shifts attributed to Chl_{D1} upon Q_A^- formation, indicates that in the T179H-PSII and in the WT*3-PSII, the Chl_{D1} itself is the chlorophyll that is first damaged by $^1O_2$, whereas in the T179V-PSII a more red chlorophyll is damaged, the identity of which is discussed. Thus, Chl_{D1} appears to be one of the primary damage site in recombination-mediated photoinhibition. Finally, changes in the absorption of Chl_{D1} very likely contribute to the well-known electrochromic shifts observed at ~430 nm during the S-state cycle.

Introduction

Oxygenic photosynthesis provides the main input of energy into biology. This process produces food, fibers and fossil fuels, and energizes the atmosphere with O_2. Photosystem II (PSII), the water-oxidizing enzyme of the cyanobacteria, algae and higher plants is at the heart of oxygenic photosynthesis. In cyanobacteria, the PSII complex comprises 17 trans-membrane and 3 extrinsic membrane proteins. These 20 subunits bind 35 chlorophylls, 2 pheophytins, 2 hemes, 1 non-heme iron, 2 plastoquinones (Q_A and Q_B), the Mn_4CaO_5 cluster, 2 Cl^-, 12 carotenoids and 25 lipids [1,2]. Sequential excitations of PSII allow the Mn_4CaO_5 cluster to accumulate oxidizing equivalents. The Mn_4CaO_5 cluster thus cycles through five redox states denoted S_n, where *n* stands for the number of stored oxidizing equivalents [3,4]. Upon formation of the S_4-state, two molecules of water are oxidized, the S_0-state is regenerated and O_2 is released.

The conversion of solar energy into chemical energy typically involves the absorption of a photon by one of the chlorophylls in the antenna. The resulting excitation is transferred to the photochemical trap which absorbs close to 680 nm, P_{680}, and which includes the four chlorophyll *a* molecules, P_{D1}, P_{D2}, Chl_{D1}, Chl_{D2} (Figure 1A). The X-ray crystal structure at 1.9 Å resolution [1,2] shows that the ligands of the Chl pigments are not identical. Most of the chlorophylls bound to PSII have histidine ligands to their Mg^{2+} ions, these include P_{D1} and P_{D2} with the D1/H198 and D2/H197, respectively, (Fig. 1B). The Chl_{D1} and Chl_{D2} are unusual in that they have water as ligands to their Mg^{2+} ions (Fig. 1C). The structures around the water ligands of Chl_{D1} and Chl_{D2} however are not identical; the water ligand to Chl_{D1} is hydrogen bonded to D1/T179, while the water ligand to Chl_{D2} is not involved in H-bonding, with the residue corresponding to D1/T179 being D2/I178, which is unable to accept a H-bond (Fig. 1C).

A role for Chl_{D1} as the primary donor was suggested in the 1980s based on evidence from comparative spectroscopy, reviewed in [5,6], and has gained support from spectroscopic studies of site-directed mutants [7-9] (see below) and from ultrafast spectroscopy [10-12]. Strong support was also provided by the recent finding that long-wavelength photochemistry can take place in chlorophyll *f*-containing PSII thanks to the presence of a single long-wavelength chlorophyll in the heart of the reaction centre located at the position of Chl_{D1} [5].

The involvement of the Chl_{D1} and Chl_{D2} in the charge separation process, reviewed in [6], was investigated by individually modifying their spectral properties in site-directed

mutants. In a study of the D1/H198Q and D2/H197N site-directed mutants in *Synechocystis* PCC 6803 it was proposed that at temperatures below 77 K, Chl_{D1} was a long-wavelength trap located at 684 nm, whereas at higher temperatures P_{D1} progressively shared more of the excitation and thus becomes more involved in the charge separation [7]. In a further study, the D1/T179 residue, which is in the close vicinity of Chl_{D1} (Fig. 1C), was replaced by either a histidine or a glutamate [7,8]. A spectroscopic characterization of these mutants confirmed that the triplet state, produced upon charge recombination from $^3[P_{680}{}^+Pheo^-]$, was localized on Chl_{D1} [7,8] as previously shown by EPR [13] and infrared spectroscopy [14]. The band at 673 nm, which mainly originates from P_{D1} and which is bleached in the difference spectrum, was unaffected in the D1/T179H and D1/T179E mutants. In contrast, the electrochromic band-shift, with a positive peak at 679 nm and a negative peak at 683 nm in the wild type sample, was blue-shifted by 1 nm in the D1/T179E mutant and red-shifted by 2-3 nm in the D1/T179H mutant [8]. This band shift was therefore attributed to the Q_Y band of $Chl_{D1,}$ which is electrochromically shifted in response to the formation of the $P_{680}{}^+Q_A{}^-$ state. The red-shift of the absorbance spectrum of Chl_{D1} in the D1/T179H mutant has been proposed to originate from an electronic polarizability of the π-system of the imidazole moiety of D1/H179 stabilizing the excited state of Chl_{D1} [7].

It is widely agreed that the Chl_{D1} has the lowest site energy of the core chlorophylls at helium temperature, *e.g.* [15] and references therein, and simulations are able to predict the spectral change in the D1/T179H mutant [16]. At room temperature, the excited state is more distributed on the six core pigments and it is predicted that $*Chl_{D1}$ remains the longest wavelength species and thus the slightly preponderant state. In agreement with that, two kinetically distinct steps are observed in the charge separation process at 77 K, *e.g.* [11] and references therein. The fastest one occurring in ~ 1 to 5 ps time range attributed to the $*[Chl_{D1}Pheo_{D1}] \rightarrow Chl_{D1}{}^+Pheo_{D1}{}^-$ reaction [11] (see [12] for work done at room temperature) whereas that occurring in 25-30 ps time range corresponds to the $*[P_{D1}Chl_{D1}] \rightarrow P_{D1}{}^+Chl_{D1}{}^-$ reaction [11].

The non-radiative charge recombination process occurs *via* different routes (reviewed in [17-19]); *i*) the pathway involving the formation of the $^3Chl_{D1}$ triplet state from the $P_{680}{}^+Pheo_{D1}{}^-$ radical pair [20], *ii*) the direct and indirect routes, between $P_{680}{}^+$ and $Q_A{}^-$ [21,22]. In a small fraction of centers, the charge recombination occurs *via* the population of a luminescent state [21]. The luminescent state it thought to be shared over all the chlorophylls of PSII, see [23] for a recent discussion, but the identity of the first excited stated formed by the back reaction has received little attention from researchers and has remained relatively

undefined. However, based on the super-luminescence of the chlorophyll *f*-containing PSII, it was recently suggested that *Chl_{D1} is likely to be the luminescent state formed from recombination of the $Chl_{D1}^{+}Pheo^{-}$ radical pair [5]. It was suggested that the *Chl_{D1} would be the first excited state formed upon radiative recombination not only in the long wavelength variant PSII but also in normal PSII [5]. This suggestion has yet to be tested.

In order to obtain new insights on the involvement of Chl_{D1} in electron transfer processes and how the nature of the Chl_{D1} ligand may affect its properties, two site-directed mutants in the thermophilic cyanobacterium *Thermosynechococcus elongatus* have been designed. The first one was D1/T179H, in which the possibility is provided for the Mg^{2+} of Chl_{D1} to have a histidine as a ligand, as for most of the other chlorophylls. The second was D1/T179V, which would eliminate the possibility for the water that ligands the Mg^{2+} to donate a H-bond to the threonine, this would mean the liganding environment for Chl_{D1} would be similar to that of Chl_{D2} (Fig. 1C). These mutants, which were both fully active for O_2 evolution, were characterized by a combination of techniques (EPR, FTIR, fluorescence and absorption spectroscopies at room temperature and 77 K, time-resolved UV-vis absorption spectroscopy, polarography and thermoluminescence) and several insights were gained concerning the primary reactions of PSII and also the initial sites of photodamage under high light.

Material and Methods

Construction of the T179H and T179V mutants and Photosystem II preparation

The *T. elongatus* strain used was the *ΔpsbA*$_1$, *ΔpsbA*$_2$ deletion mutant [24], called WT*3, constructed from the *T. elongatus* 43-H strain that had a His_6-tag on the carboxy terminus of CP43 [25]. For the construction of the D1/T179H and D1/T179V site-directed mutants, the positions around +533 from the initial codon of *psbA*$_3$ ORF were substituted on a plasmid DNA in order to introduce the T179H and T179V substitutions and to create restriction sites for *Msc* I and *Bsa*H I, respectively, by a Quick–Change Lightning Site–Directed Mutagenesis Kit (Agilent Technologies) as shown in Fig. 2A. After introduction of the plasmid DNA into the host cells by using a Gene Pulser (BioRad), mutant cells were selected from the cells on DTN agar plate containing 5 µg mL^{-1} of chloramphenicol, 6 µg mL^{-1} of gentamycin (Gm), and 40 µg mL^{-1} of kanamycin. Fig. 2C shows the results of the genomic DNA analyses around site-directed mutation of segregated cells. After PCR amplification of the mutated region by using a forward primer (Fw; 5'–

CTACAACGGTGGCCCCTACCAACTG–3') and a reverse primer (Rv; 5'–GCTGATACCCAGGGCAGTAAACCAGATGCC–3') (Fig. 2B), the PCR products were digested with *Msc* I or *Bsa*H I for T179H and T179V, respectively. As shown in Fig. 2C, amplified a 554-bp DNA fragments (Fig. 2C, lanes 2 and 4) were completely digested with *Msc* I for separation into a 216 bp and a 338 bp or *Bsa*H I for separation into a 215 bp and a 339 bp for T179H (lane 3) and T179V mutants (lane 5), respectively. Then, the genomic DNA sequence of the open reading frame of $psbA_3$ was confirmed by nucleotides sequencing by using a GenomeLab GeXP DNA sequencer (Beckman Coulter).

PSII purifications were achieved as previously described [26]. PSII were suspended in 1 M betaine, 15 mM $CaCl_2$, 15 mM $MgCl_2$, 40 mM MES, pH 6.5 then frozen in liquid nitrogen until use.

SDS-polyacrylamide gel electrophoresis

Purified PSII (8 µg Chl each) suspended in 40 mM MES/NaOH (pH 6.5), 10 mM NaCl, 10 mM $CaCl_2$, 10 mM $MgCl_2$, 0.03% *n*-dodecyl-β-D-maltoside were solubilized with 2% lithium laurylsulfate, and then analyzed by an SDS-polyacrylamide 16–22% gradient gel electrophoresis containing 7.5 M urea as previously described [27].

Oxygen evolution and consumption

Oxygen evolution was measured under continuous illumination at 25°C by polarography using a Clark-type oxygen electrode (Hansatech) with saturating white light through infrared and water filters. For O_2 evolution, the initial activity was measured in the presence of 0.5 mM 2,6-dichloro-*p*-benzoquinone, dissolved in dimethyl sulfoxide (DMSO), as an electron acceptor. The medium used contained 20 mM MES, 15 mM $CaCl_2$, 15 mM $MgCl_2$, 20 mM NaCl, pH 6.5.

Singlet oxygen production

Singlet oxygen production was detected by histidine mediated oxygen uptake measurements under high light illumination conditions (20,000 µmol photons m^{-1} s^{-1}) at 25°C, as previously described in [28, 29]. The activity was measured in 20 mM MES buffer (pH 6.5) containing 15 mM $CaCl_2$, 15 mM $MgCl_2$, 20 mM NaCl in the presence of 10 mM L-histidine and 25 µM DCMU (3-(3,4-dichlorophenyl)-1,1-dimethylurea) at chlorophyll concentration of 5 µg mL^{-1} by using a Clark-type oxygen electrode (Hansatech).

EPR spectroscopy

X-band cw-EPR spectra were recorded with a Bruker Elexsys 500 X-band spectrometer equipped with a standard ER 4102 (Bruker) X-band resonator, a Bruker teslameter, an Oxford Instruments cryostat (ESR 900) and an Oxford ITC504 temperature controller. The S_2 multiline state was induced by illumination with an 800 W tungsten lamp filtered by water and infrared cut-off filters was used. Illuminations for approximately 5-10 seconds at temperatures close to 198 K in a non-silvered Dewar in ethanol cooled with dry ice. The triplet state was measured under illumination at 4.2 K inside the EPR cavity. The illumination was done with a low voltage halogen lamp (Philips GX5.3, 24 V, 250 W) filtered by water and infrared cut-off filters.

PSII samples were loaded in the dark into quartz EPR tubes at 1.1 mg of Chl mL^{-1} and dark-adapted for 1 h at room temperature. The samples were then synchronized in the S_1-state with one pre-flash [30]. Flash illumination at room temperature was provided by a neodymium:yttrium–aluminum garnet (Nd:YAG) laser (532 nm, 550 mJ, 8 ns Spectra Physics GCR-230-10). After a further 1 h dark-adaptation at room temperature the samples were frozen in the dark to 198 K in a dry-ice/ethanol bath and then transferred into liquid N_2, (77 K). Prior to recording the spectra the samples were degassed at 198 K.

Thermoluminescence measurements

Thermoluminescence (TL) glow curves were measured with a lab–built apparatus [31,32]. Purified PSII were diluted to 10 µg Chl mL^{-1} in 1 M betaine, 40 mM MES, 15 mM $MgCl_2$, 15 mM $CaCl_2$, pH 6.5 and then dark-adapted for 1 h at room temperature before the addition of 10 µM DCMU. Flash illumination was done at 0°C by using a saturating xenon flash. One second after the flash illumination, the samples were heated at the constant heating rate 0.7°C/s and TL emission was detected. It was verified that after the dilution the PSII samples had the same OD at 673 nm.

UV-visible time-resolved absorption change spectroscopy

Absorption changes measurements were measured with a lab-built spectrophotometer [33], in which the absorption changes are sampled at discrete times by short analytical flashes. These analytical flashes were provided by an optical parametric oscillator pumped by a frequency tripled Nd:YAG laser, producing monochromatic flashes (355 nm, 1 nm full-width at half-maximum) with a duration of 5 ns. Actinic flashes were provided by a second Nd:YAG laser (532 nm), which pumped an optical parametric oscillator producing

monochromatic saturating flashes at 700 nm with the same flash-length. The path-length of the cuvette was 2.5 mm. PSII was used at 25 µg of Chl mL^{-1}. PSII samples were diluted with a solution containing 1 M betaine, 15 mM $CaCl_2$, 15 mM $MgCl_2$, and 40 mM MES (pH 6.5). PSII samples were dark-adapted for ≈ 1 h at room temperature (20–22°C) before the addition of 0.1 mM phenyl *p*–benzoquinone (PPBQ) dissolved in DMSO.

77 K Absorption spectra

Low temperature absorption spectra were recorded using a spectrophotometer U-3900H (Hitachi High Tech. Co., Japan) equipped with a cryostat Optistat CF (Oxford Instruments) for low temperature measurements and with a cw lamp (MSG3-1100S-SD; Moritex Co., Japan) for illumination. For the light-*minus*-dark difference absorption spectra recorded at ~ 77 K, dark-adapted PSII at 0.1 mg Chl mL^{-1} were illuminated for 30 s with a ≈ 30 mW cm^{-2} light source filtered by infrared and UV cut-off filters. The PSII cores were in 20 mM MES buffer (pH 6.5) containing 15 mM $CaCl_2$, 15 mM $MgCl_2$, 10 mM NaCl and 65% glycerol. The wavelength accuracy was ± 0.1 nm, the spectral band-pass was 2 nm and the scan speed was 60 nm min^{-1} or 300 nm min^{-1} for 600 to 750 nm or 350 nm to 800 nm, respectively.

For measurements of the difference spectra after-*minus*-before high light illumination, PSII samples suspended in 20 mM MES buffer (pH 6.5), 15 mM $CaCl_2$, 15 mM $MgCl_2$, 10 mM NaCl, and 0.5 M mannitol at a concentration of 6.5 µg Chl mL^{-1} were illuminated at 45°C with a light intensity of ≈ 500 µmol photons m^{-2} s^{-1} for 60 min. After the high light illumination, PSII samples were concentrated by using Amicon Ultra-0.5 (Millipore Corp.) and resuspended in 20 mM MES, 15 mM $CaCl_2$, 15 mM $MgCl_2$, 10 mM NaCl and 65% glycerol buffer (pH 6.5) for measurements at ≈ 77 K.

Room temperature absorption spectra were recorded using a spectrophotometer U-3900 (Hitachi High Tech. Co., Japan). The wavelength accuracy was ± 0.2 nm, the spectral band-pass was 2 nm and the scan speed was 120 nm min^{-1}.

77 K Fluorescence spectra

Fluorescence emission spectra of cells were recorded at ~ 77 K using a Fluorescence spectrophotometer F-2700 (Hitachi High Tech. Co., Japan) as previously described in [34]. PSII samples were suspended in 20 mM MES (pH6.5) containing 20 mM NaCl and 200 mM mannitol at 5 µg Chl mL^{-1}. The PSII were illuminated in liquid N_2 at 440 nm with a resolution

of 20 nm. The fluorescence emission spectra were measured with the scan speed of 300 nm min^{-1} with a resolution of 2.5 nm.

FTIR measurements

Light-induced P_{680}^{+}/P_{680} FTIR difference spectra were measured using a Bruker VERTEX 80 spectrophotometer following the method described previously [35]. An aliquot of the PSII suspension was mixed with 1 µL of 500 mM potassium ferricyanide and 1 µL of 10 mM SiMo on a CaF_2 plate, lightly dried under N_2 gas flow, and covered with another CaF_2 plate with 0.7 µL of water. The sample temperature was adjusted to 265 K in a cryostat (Oxford, model DN1704). Single-beam spectra with 1-s scans were recorded under dark and during illumination, and the measurement was repeated 5000, 4000, and 2000 times for the WT*3-PSII, T179H-PSII, and T179V-PSII samples, respectively.

Results

Intactness of the mutant PSII

The *T. elongatus* D1/T179H and D1/T179V mutant cells were able to grow photo-autotrophically under moderate light intensity (≈ 50 µmol photons m^{-2} s^{-1}), although the T179V mutant cells were more sensitive to very high light conditions (≈ 200 µmol photons m^{-2} s^{-1}), see Fig. S1. Active PSII could be purified from both types of mutant cells. The oxygen evolution activity of isolated PSII from WT*3, T179H and T179V was ≈ 3500 µmol O_2 (mg Chl)$^{-1}$ h^{-1}, ≈ 3500 µmol O_2 (mg Chl)$^{-1}$ h^{-1}, and ≈ 2500 µmol O_2 (mg Chl)$^{-1}$ h^{-1}, respectively. No loss of subunits in isolated PSII in either of the mutants was detected by SDS-polyacrylamide electrophoresis (not shown). Fig. 3 shows the amplitude of the absorption changes at 292 nm induced by each flash of a sequence given to dark-adapted samples and recorded in the WT*3-PSII (black points), the T179H-PSII (red points) and the T179V-PSII (blue points). Measurements were done 100 ms after the flashes, *i.e.* after the reduction of $Tyr_Z^{\bullet}$ by the Mn_4CaO_5 cluster was complete [36,37]. This wavelength corresponds to an isosbestic point for $PPBQ^{-}$/PPBQ, the added electron acceptor, and is in a spectral region where the absorption of the Mn_4CaO_5 cluster depends on the S_n-states [37]. No significant

differences in the oscillating pattern are observed between the two PSII mutants and the WT*3-PSII thus confirming that both mutants are fully active.

In *Synechocystis* 6803, the absorption spectrum at ~ 77 K of the T179H-PSII mutant in the Q_Y region has been found to be slightly modified with a decrease in the absorption around 682 nm [8]. A similar decrease at 682 nm was also observed in the *T. elongatus* T179H mutant (see Fig. S2A). Fig. 4 shows the effect of a continuous illumination at ~ 77 K in WT*3-PSII, T179V-PSII and T179H-PSII. Under these conditions, the side-path donors expected to be oxidized are either Car, Chl_Z or Cytb_{559} and the dominant reduced electron acceptor formed is Q_A^-, *e.g.* [38-40]. The light-*minus*-dark absorption spectra recorded at ~ 77 K from 350 nm to 800 nm is shown in Fig. S2B. Panels A and B in Fig. 4 shows the light-*minus*-dark absorption spectra with an expanded wavelength scale in two specific regions. Panel A (see also Fig. S3) shows the spectral region from 520 nm to 570 nm, which includes the electrochromic blue shift of the $Pheo_{D1}$ Q_X absorption induced by the formation of Q_A^- and known as the C-550 shift. This band-shift was centered at ~ 547 nm in the 3 samples, a wavelength that is characteristic of the presence of the hydrogen bond from D1/E130 to the ^{1}13-keto group of $Pheo_{D1}$ which occurs when D1 is PsbA3 in WT*3-PSII (Fig. 1A), *e.g.* [26,41] and references therein. A bleaching centered at 557-558 nm was also observed in the 3 samples. This corresponds to the α-band of Cytb_{559} which decreased in intensity upon the oxidation of the cytochrome as expected upon an illumination at 77 K. Data in Fig. S3 shows a more oxidation of Cytb_{559} in both mutants under the 77 K continuous illumination.

Panel B in Fig. 4 shows the reaction center Q_Y electrochromisms upon Q_A^- reduction [41]. One band shift (the red-shift) was centered at ~ 678 nm in the WT*3-PSII. This band shift mainly originates from the effect of the formation of Q_A^- on the absorption of the $P_{D1}P_{D2}$ pair in the ground state [42,43]. This band shift was not significantly modified in the D1/T179 mutants thus showing that the mutations of T179 did not affect the absorption of $P_{D1}P_{D2}$. The second band shift (a blue-shift) corresponds to the change in the absorption of Chl_{D1} upon Q_A^- formation. This band shift was centered at ~ 686 nm in WT*3-PSII and was red-shifted by ~ 3 nm to ~ 689 nm in the T179H-PSII. The red-shift of this band shift is very similar to that observed upon the formation of $(P_{D1}P_{D2})^+Q_A^-$ in *Synechocystis* 6803 [8,9] where a shift from 682 nm to ~ 685 nm was reported. In contrast, in the T179V-PSII, the band shift attributed to Chl_{D1} seemed to be not significantly modified. Interestingly, a blue-shift of the negative part of the differential signal at 676-677 nm was observed in the D1/H198Q mutant upon Q_A^- formation (green spectrum). A blue shift of the bleaching corresponding to the P^+ formation was also observed in such a mutant [7,24].

Time-resolved flash-induced absorption changes in the Soret region

In the present work, the effect of the mutations on the $P_{680}^{+}Q_A^{-}$-*minus*-$P_{680}Q_A$ difference spectrum was also measured at room temperature, Fig. 5, by recording the time-resolved flash-induced absorption changes around 430 nm. In this spectral region, the redox changes of several species, such as the Chls, cytochromes, Tyr_Z and Q_A, give rise to absorption changes. The most prominent of these, however, is a strong Soret band bleaching in the 433 nm region associated with the formation of P_{680}^{+}. In Fig. 5, the absorption changes were measured 5 ns after the first flash given to dark-adapted PSII *i.e.* in the S_1-state, and therefore corresponded to the $S_1Tyr_ZP_{680}Q_A$ to $S_1Tyr_ZP_{680}^{+}Q_A^{-}$ transition. Although no major differences were detected between the WT*3-PSII and the two mutants at room temperature, the spectra appeared very slightly broader in the two mutants (~ 1 nm), with a broadening to the red in the T179H-PSII and to the blue in the T179V-PSII. The same results were obtained after averaging the spectra recorded on the first four flashes (see Fig. S4).

Fig. 6A shows the triplet EPR signal [20] known to be localized on Chl_{D1} [13,14]. The difference spectra are the light spectra measured under continuous illumination at 4 K *minus* the spectra recorded in the dark after the illumination. The triplet signal has the same spin polarization in the two mutants when compared to the WT*3-PSII. The extra signal present in all samples at around 3550 gauss does not arise from the triplet signal. This unidentified EPR signal is often detected in the His-tag PSII in the presence of a high amount of dithionite as is the case here [44] but was also detected in PSII from *Synechocystis* 6803 which had no His_6-tag [45]. Fig. 6B and 6C show the external resonances with an expanded magnetic field scale. Although the triplet EPR signal is not expected to be very sensitive to the environment of the ^{3}Chl species, *e.g.* [20,45-48], the spectral changes detected in Fig. 6 show that the modifications in the environment of the $^3Chl_{D1}$ in the T179H-PSII mutant became detectable with the total width of the signal smaller by ~ 10 gauss. This narrowing could reflect a change from water to His as the Chl_{D1} ligand in the D1/T179H mutant. Indeed, the $^3P_{700}$ EPR signal is slightly narrower than the $^3Chl_{D1}$ EPR signal [49], and P_{700} has His ligands [50]. The T179V mutant seems to have a different proportionality for the Z peaks compared to the Y and X peaks. This could indicate a change in the relative lifetimes of the triplet sublevels: either the "Z" sublevel got faster or the "X" and "Y" sublevels got slower.

The intactness of the Mn_4CaO_5 cluster in the T179H-PSII and T179V-PSII allowed us to study the charge recombination process by thermoluminescence in these mutants. Fig. 7 shows the TL curves, in the presence of DCMU, resulting from the $S_2Q_A^{-}$ charge

recombination recorded in WT*3-PSII (black curve), T179H-PSII (red curve) and T179V-PSII (blue curve). In the WT*3-PSII the peak was at 31°C. In the T179V-PSII, the peak temperature was decreased to 24°C with a slight decrease in the area. In the T179H-PSII, the peak of the TL band was further down shifted to ~ 14°C with a dramatic decrease of the area. The small amplitude of the TL curve in the T179H-PSII was the reason to use a fast heating rate in this study, *i.e.* 0.7°C/s. Indeed, with slower heating rates the signal became undetectable. As a consequence of this high heating rate, the peaks appeared at temperatures higher than those generally reported for the $S_2Q_A^-$/DCMU charge recombination in *T. elongatus* [24,26].

A change in the energy level of the radical pairs populated during the charge recombination process can be tested for by looking at the charge recombination rates which mainly depend on the direct and indirect routes, involving either P_{D1}^+ or Chl_{D1}^+. Fig. 8 shows the low spin, $S = 1/2$, S_2 multiline EPR signal recorded after an illumination at 200 K given to WT*3-PSII (panel A), T179H-PSII (Panel B) and T179V-PSII (Panel C). The spectra shown in black are the light-*minus*-dark spectra recorded immediately after the illumination at 200 K. The vertical scales in the 3 panels are identical, which makes the amplitude of the spectra comparable. A similar amount of S_2 was induced in the 3 samples since no high-spin S_2 signals were detected in any of the 3 samples in the conditions used here (not shown). The amplitude of the $Q_A^-Fe^{2+}Q_B^-$ signal at $g = 1.66$ (~ 4000-4200 gauss) [51,53] induced by the 200 K illumination in the absence of an added electron acceptor was also similar in the 3 samples thus showing that the amount of $Q_AFe^{2+}Q_B^-$ prior to the illumination was similar. The addition of DCMU in the dark-adapted PSII mutants was therefore not expected to result in a different proportion of closed centers in the $Q_A^-Fe^{2+}$/DCMU state prior to the flash illumination in the TL experiment reported above. The spectra in red are the light-*minus*-dark spectra for which the light spectra were recorded after a further dark period of 5 minutes at ~ 20-22°C following the illumination at 200 K. In WT*3-PSII, approximately 60-70 % of the multiline was still detected after the 5 minutes at room temperature, whereas in the T179V-PSII and T179H-PSII less than 40 % and 10 %, respectively, were detected. The TL signal originating for the $S_3Q_B^-$ charge recombination was also monitored after two flashes (Fig. S5) with similar effects of the mutations on the peak temperature and TL amplitude to those seen in Fig. 7. Upon a further dark-period of 5 minutes following the 2 flash illumination, the TL signal was smaller in the mutants becoming almost undetectable in the T179H-PSII. The results of these experiments are consistent with the more efficient non-radiative charge recombination in the two mutants, particularly in the T179H-PSII.

The ability of the mutants with modified Chl_{D1} properties to evolve O_2 prompted us to study to what extent the mutations may affect the production of reactive oxygen species, in particular the singlet $^1O_2$ known to be formed by the reaction of $^3O_2$ with $^3Chl_{D1}$. By using the protocol described by Rehman et al. [28] the data in Fig. 9A shows that under the high light illumination used in this study, the $^3O_2$ consumption that is assumed to be proportional to the production of $^1O_2$ [28,29], was 163 µmol (mg Chl)$^{-1}$ h^{-1}, 148 µmol (mg Chl)$^{-1}$ h^{-1} and 227 µmol (mg Chl)$^{-1}$ h^{-1} in WT*3, T179H and T179V, respectively. Therefore, the $^1O_2$ release under the high light illumination was decreased by ~ 10% in the T179H-PSII and enhanced by ~ 40% in the T179V-PSII. Panel B in Fig. 9 shows that under high light illumination the chlorophyll bleaching was also slightly larger in the T179V-PSII and slightly smaller in the T179H-PSII. This result suggests that the bleaching could be, at least in part, correlated to the amount of $^1O_2$ produced. Fig. 9C and 9D show the difference spectra "after-*minus*-before" room temperature high light illumination, measured at 77 K and room temperature, respectively. They show the bleached species with an expanded scale in the Q_Y region of Chl *a* (all spectra in Panels C and D have been normalized to the same amplitude). In both mutants the red-shift of the spectra indicates that some of the bleached chlorophyll(s) exhibit a spectrum slightly red-shifted compared to the bleached Chl in the WT*3-PSII. By comparison with the amplitude of the bleaching in WT*3-PSII, the difference spectra appeared slightly broader and slightly bigger above 673 nm, particularly in the T179V-PSII in which the shoulder at 683.5 nm seemed more pronounced.

Fluorescence spectra at 77 K

At 77 K, the fluorescence emission at 695 nm has been proposed to arise from the longest wavelength CP47 chlorophyll, whereas the emission at 685 nm has been assigned to arise from chlorophyll(s) absorbing at 683nm in CP47 and CP43, which transfer excitation slowly to the photochemical heart of the reaction center [54]. Fig. 10 shows that the fluorescence spectra at ~ 77 K were also affected in the two mutants studied here with a shift of the main peak from 686.5 nm in WT*3-PSII to 687.5 nm in T179H-PSII and an increase in the fluorescence at ~ 695 nm in the T179H-PSII and a decreased 695 nm fluorescence in the T179V-PSII.

Electrochromism in the Soret region

The oxidation/reduction and protonation/deprotonation reactions on the electron donor side of PSII are also known to change the electrostatic environment of the chlorophylls,

shifting their absorption spectra with the size and direction of the shifts depending on the distance and orientation of the chlorophyll relative to the location of the charge [37,55,56]. In plant PSII, electrochromic shifts in the blue region of the chlorophyll spectrum and their pH dependence have been reported for the S_1 to S_2, S_2 to S_3 and S_0 to S_1 transitions [37,55] and, from the positions of the peaks and troughs of the electrochromic shifts, it has been found that the amplitude of the 428 nm-*minus*-440 nm in a flash sequence oscillated with a period of four. The identity of the chlorophyll(s) sensitive to the redox state of the Mn_4CaO_5 cluster however remains to be determined.

Panel A in Fig. 11 shows the difference spectra induced by each of the first 6 flashes given to dark-adapted WT*3-PSII. These spectra recorded 100 ms after the flashes, *i.e.* when only the charge on the Mn_4CaO_5 cluster contribute, are comparable to those recorded in plant PSII [37]. Panel B in Fig. 11 shows the amplitude of the difference, 428 nm-*minus*-440 nm, after each flash of a sequence given to dark-adapted samples and recorded in the WT*3-PSII (black), in the T179H-PSII (red) and in the T179V-PSII (blue). As shown in Fig. 3 for the measurements at 292 nm, the oscillations with a period of four are clearly detectable at least until the 20^{th} flash and no significant differences in the oscillating pattern were observed between the two PSII mutants and the WT*3-PSII except for the first flash.

In the work done on plant PSII [37,55] the spectra were recorded in the presence of carbonyl cyanide *p*-(trifluoromethoxy)-phenylhydrazone (FCCP), which is an accelerator of the deactivation of the S-states [37]. The presence of FCCP allowed several sequences on the same sample to be recorded by shortening the duration of a complete dark-adaptation. Consequently, in the published work [37,55] the first flash data contained no or smaller contributions from centres that remain in S_1 after the first flash (*i.e.* from either $S_1Tyr_D \rightarrow S_2Tyr_D \rightarrow S_1Tyr_D^{\bullet}$ or the less likely [57] $S_0Tyr_D^{\bullet} \rightarrow S_1Tyr_D^{\bullet}$ transitions). Note that these reactions are also eliminated by the pre-flash protocol in the EPR experiments reported above. The protocol using FCCP in plant PSII was prone to complications due to secondary effects and much time and effort was needed to avoid them [37,55], thus the use of FCCP was avoided in the present work on *T. elongatus*. Moreover, although the signal on the first flash in Panel B of Fig. 11 differs in the mutants when compared to the WT*3-PSII in this spectral region, the similar amplitude of the oscillations on the following flashes shows that the spectral difference was mainly limited to the first flash as previously observed [37].

Panel C in Fig. 11 shows the difference spectra recorded on the third flash, *i.e.* in the transition in which the electrostatic constraints are relaxed since the enzyme cycle has returned to the lowest redox state (S_0) in the majority of centers. The black spectrum was

recorded in WT*3-PSII, the red spectrum in T179H-PSII and the blue spectrum in T179V-PSII. Two observations can be made: *i*) in WT*3-PSII, the spectrum very likely contained two spectral components, and *ii*) the difference spectra in the two mutants were similar and slightly differed from that in WT*3-PSII.

Discussion

The oscillating patterns at 292 nm in Fig. 3 show that both the T179H-PSII and the T179V-PSII mutants were fully active at room temperature. The similar amplitude of the S_2 multiline EPR signal formed at 200 K in the WT*3-PSII and the two mutants shows that the S_1 to S_2 transition at 200 K also remained unaffected by the mutations (see Fig. 8). The similar amplitude of the $Pheo_{D1}$ band-shift at 550 nm upon illumination at 77 K, which is proportional to the amount of Q_A^- present, shows that the charge separation remained similarly efficient at 77 K in both mutants and in the WT*3-PSII (see Fig. 4A).

The light-minus-dark absorption spectra recorded at 77 K are almost identical to those recorded earlier at 8 K in WT*3-PSII [41], see also Fig. S3. As the time-resolved 550 nm band-shift from $Pheo_{D1}$ was recorded at room temperature, it was significantly broader than those in the literature recorded at low temperatures, although the band-shift was centered at the same wavelength, which is characteristic of PSII in which D1 is PsbA3 (see Fig. S2B and Fig. S3). The full light-*minus*-dark absorption spectra, Fig. S2B, exhibits some bands below 550 nm showing that the oxidation of a carotenoid also occurred in a proportion of centers in addition to the oxidation of Cytb_{559}.

The data in Fig. 4B show that the band-shift centered at ~ 686 nm in WT*3-PSII which is attributed to a blue-shift of the Chl_{D1} absorption upon Q_A^- formation, was red-shifted by ~ 3 nm to ~ 689 nm in the T179H-PSII. This shift to longer wavelength is very similar to that observed upon the formation of $P_{D1}^+Q_A^-$ in *Synechocystis* 6803 by time-resolved measurements under flash excitation at 77 K [8,9]. In contrast, in the T179V-PSII, the Chl_{D1} band-shift was not significantly modified compared to the WT*3-PSII.

The spectral features at shorter wavelengths (the red-shift centered at ~ 678 nm, the blue shift at 674 nm and the possible red-shift at 664 nm), which presumably arise from the other reaction center pigments, including P_{D1} and P_{D2} [15,42], underwent no or minor modifications in terms of their wavelength position in the T179H and T179V mutants. This agrees with the earlier report of a lack of spectroscopic changes associated with P_{D1} in the $P_{D1}^+Q_A^-$ difference spectra caused by the T179H mutation [8,9].

At room temperature, the time-resolved P_{680}^+ spectra (see Fig. 5) appeared to be slightly broadened in the two mutant PSII when compared to WT*3-PSII. This broadening could suggest a very slight increase of the proportion of the $P_{D1}^+P_{D2}$ state in T179H-PSII and a very slight increase of the $P_{D1}P_{D2}^+$ state in T179V-PSII when compared to the WT*3-PSII [58]. However the P_{680}^+-*minus*-P_{680} FTIR difference spectra also recorded at 265 K (see Fig. S6) did not show a change in the ratio of the amplitude of the positive bands at 1724 cm^{-1} and 1709 cm^{-1} attributed to the asymmetric distribution of a positive charge on P_{D1} and P_{D2}, respectively [34]. Thus it seems that the P_{D1}^+/P_{D2}^+ ratio was not significantly affected by the mutations. In agreement with that, the electron transfer from Tyr_Z to P_{680}^+ also remained unaffected in the mutants, see Fig. S4B. The data above show that at room temperature the $P_{680}^+Q_A^-$ state remained essentially unmodified in functional terms and in the two mutants in full agreement with the literature [8,9].

In T179H-PSII, the room temperature spectrum of the bleached Chl after high light illumination has its peak red-shifted by ~ 2 nm (see Fig. 9B and 9C). The amplitude and the direction of the shift are similar to those of the Chl_{D1} spectrum. Thus, this could indicate that in this mutant the $^1O_2$ produced by the $^3Chl_{D1} + {}^3O_2$ reaction reacts directly with Chl_{D1}. This also occurs with the WT*3-PSII, thus indicating that Chl_{D1}, the location of the triplet [13], is among the first chlorophylls to be damaged by the singlet oxygen that is generated by energy transfer from the chlorophyll triplet. The red-shift in the fluorescence maximum from 685 to 688 nm correlates with the absorption peak of Chl_{D1} in the T179H mutant, indicating that Chl_{D1} itself may be the main emitter at 77K.

For the T179V mutant, the situation seems more complex. The absorption spectrum appeared only slightly modified in both the time-resolved spectra (Fig. 5) and in terms of the Q_A^- induced band-shift at 77 K data (Fig. 4B). In contrast the chlorophyll bleached by high light was significantly red-shifted in this mutant. These effects in the T179V-PSII may be explained as follows. The high light illumination was done in non-frozen conditions, it is known that after its formation at the Chl_{D1} site, the triplet can migrate onto other chlorophylls at non-cryogenic temperatures [59]. In this mutant the migration may be favored by the symmetrization so that the triplet escapes and localizes at another chlorophyll with a low energy triplet state, in this case (one of) the lowest energy Chls, which could be the red trap in CP47. In support of this hypothesis, it has been observed in single-molecule experiments that a loss in the fluorescence emission at 695 nm could be due to the migration of the triplet to red-most chlorophylls, either Chl29 or Chl11 in CP47 [60-62]. During the lifetime of the ^{3}Chl29 triplet state, the Chl29 is not expected to contribute to the fluorescence spectrum [60].

The lower of fluorescence at 695 nm seen in the T179V-PSII could represent a similar phenomenon but enhanced by the mutation (see Fig. 10).

This model however has its weaknesses. Given the specific distance limitations of the Dexter mechanism associated with triplet transfer, triplet migration all the way to the rather distant far red antenna chlorophyll in the CP47 seems rather unlikely and we also might expect the triplet to encounter carotenoid on the way. Another explanation that seems possible is that the diminished Chl_{D1} bleaching due the mutational perturbation, simply allows the second most vulnerable site to be bleached. As the longest wavelength chlorophylls in the system, the CP47 chlorophylls are the most likely chlorophylls to be over-excited when the usual photochemistry in the reaction centre is perturbed. Indeed the long-wavelength CP47 chlorophylls are considered to represent an emission site that favors displacement of the excitation away from the centre of the reaction centre for regulation and protection [62]. This mechanism would make more sense physiologically if the excitation were quenched efficiently upon arrival at the long-wavelength emitter. The candidates for this role include PSI or carotenoids under physiological conditions; in the isolated cores it is not unlikely that putative carotenoids are removed or perturbed. Without the protective quenching, the chlorophylls acting as terminal emitters would likely be bleached by the $^1O_2$ produced by O_2 reacting with chlorophyll triplet formed at long wavelength chlorophyll on CP47.

Fig. 9A shows a correlation between the lower production of $^1O_2$ (monitored by $^3O_2$ consumption), less chlorophyll bleaching both in the absorption spectra (Fig. 9B) and greater tolerance to growth in high light (Fig. S1) in the T179H-PSII. In this mutant, charge recombination appeared much faster than in the WT*3-PSII and the T179V-PSII (see Fig. 7), which could indicate either a shorter lifetime for the $Chl_{D1}^+Pheo_{D1}^-$ state, or another faster non-radiative route that is also a non-triplet route. In turn, that could be an explanation for a smaller amount of $^3Chl_{D1}$ under these conditions and therefore less $^1O_2$. A similar relationship has been previously proposed in mutant with a modified energy level of $Pheo_{D1}$ [28].

In the Chl*f*-containing PSII from *Chroococcidiopsis thermalis* grown in 750 nm light, Chl_{D1} appears to be the only one of the six central chlorins that is changed to a long wavelength pigment (Chl*f* or less likely Chl*d*), while Chl_{D2}, P_{D1} and P_{D2} remained Chl*a*, and both pheophytins remained pheophytin *a* [5]. The TL bands arising from the $S_2Q_A^-$/DCMU and from $S_2Q_B^-$ charge recombination were enhanced by a factor >25. These data were explained by a model in which the energy gap between the luminescent excited state of chlorophyll and its precursor radical pair was smaller than in normal Chl*a*-containing PSII. The luminescent state was assigned to a long wavelength version of $^*Chl_{D1}$ (Chl*f* or Chl*d*) and

this was supported by the identification of Chl_{D1} absorbing at ~720 nm. The precursor radical pair was attributed to $Chl_{D1}^{+}Pheo_{D1}^{-}$ [5].

The situation in normal Chl*a*-containing PSII is expected to be more complex than the special case in which Chl_{D1} is at a uniquely low energy compared to the other central cofactors [5]. However in the present case, where the Chl_{D1} has been specifically modified by mutation, this recent, more detailed model [5] seems appropriate. Theoretical treatments have been developed that explain how TL is affected by changes of the energy levels of the relevant radical pairs involved in PSII back-reactions [17,63], and based on these models and on the new considerations for the luminescence mechanism [5], the much weaker TL intensity in the T179H-PSII mutant seen here can be explained. The mutation increases the energy gap between the precursor radical pair, usually taken as $P_{D1}^{+}Pheo_{D1}^{-}$ but here taken as $Chl_{D1}^{+}Pheo_{D1}^{-}$, and the luminescent state, which we consider to be mainly $^{*}Chl_{D1}$ but which in this "normal" PSII is likely to equilibrate over the rest of the chlorin pigments. This increased energy gap in the mutant suggests that a histidine ligand to Chl_{D1} may decrease the potential of the Chl_{D1}^{+}/Chl_{D1} couple.

The second effect of the T179H mutation on the TL seen in Fig. 7 was a decrease of the peak temperature by more than 15°C and an increase in the rate of charge recombination. This TL temperature decrease is taken as an indication that the final precursor radical pair (*i.e.* $Chl_{D1}^{+}Pheo_{D1}^{-}$) is more easily populated from its own precursor radical pair (*i.e.* $P_{D1}^{+}Pheo_{D1}^{-}$ in the charge recombination process, see Fig. 12). This would also fit with a lowering of the potential of the Chl_{D1}^{+}/Chl_{D1} couple (see Fig.12).

In this model there is no need to invoke changes in the E_m of components other than Chl_{D1}. While such changes cannot be ruled out they are not needed to explain the basic observations. This simple model fits well with the experimental data showing a shift in the spectrum of Chl_{D1} and no significant changes in the absorption spectra of P_{D1}, P_{D2} and $Pheo_{D1}$. The small shift in the absorption of the Chl_{D1} (3 nm) reflects a very small change in the energy (8.5 meV) of the $^{*}Chl_{D1}$ state and this is unlikely to be relevant to the mechanistic effect observed given the heat of the environment (k_BT = 26 meV).

Fig. 12 summarizes the simple model used above for the T179H-PSII. Compared to previous models, the non-radiative routes (k_i^1 and k_i^2) now involves the two states, $Chl_{D1}^{+}Pheo_{D1}^{-}$ and $P_{D1}^{+}Pheo_{D1}^{-}$ radical pairs as in the charge separation process, see [64] for a review. There are many interesting aspects of this kind of model that are worth noting and investigating but these are outside the scope of this article, which aims simply to apply the new thinking [5] to explain the basic observations in the present study. The key points are that

the decrease in the energy level of the $Chl_{D1}^{+}Pheo_{D1}^{-}$ radical pair due to modification of the Chl_{D1} environment results in less luminescence and a lower temperature TL peak. It also could be consistent with less chlorophyll triplet formation (Fig. 9A) resulting in less photodamage (Fig. 9B) *in vitro* and therefore possibly *in vivo*.

In the T179V-PSII mutant the TL was less affected than in the T179H-PSII. From the down-shift of the TL peak temperatures, the decrease of the energy level of the $Chl_{D1}^{+}Pheo_{D1}^{-}$ state in the T179V-PSII relative to that of the wild type PSII seemed to be approximately half of that in the T179H-PSII mutant. However, from the amplitude of the TL signal the energy gap between the $Chl_{D1}^{+}Pheo_{D1}^{-}$ state and $^{*}Chl_{D1}$ seemed only slightly affected in the T179V-PSII. In contrast, the site of damage as manifest by bleaching seems to be shifted to the long wavelength chlorophyll in CP47 as discussed above. The mechanistic link between the perturbation at the level of Chl_{D1} and resulting bleaching on the CP47 chlorophyll has yet to be established.

In plant PSII, an electrochromic shift in the blue region and its pH dependence has been reported for the S_1 to S_2, S_2 to S_3 and S_0 to S_1 transitions [36,55]. However, the chlorophyll(s) involved remained to be fully identified. The electrochromic shift of a pigment, here a chlorophyll, depends on the orientation of the chromophore, the distance between the chromophore and the charge, and the nature (positive, negative) and intensity of the charge, *e.g.* [5,56]. It is therefore not surprising that the spectra in Fig. 11 contain more than one component taking into account the complex electron and proton events in the S-state cycle, in particular in the S_3 to S_0 transition. The important point that we want to address here is that in the two mutants, the broader components became narrower and underwent a slight red-shift, by ~ 1 nm, of the electrochromic band-shift. Since Chl_{D1} is a pigment which has a modified absorption in the mutants, at least in the T179H-PSII, the results above suggest that Chl_{D1} could be the chlorophyll that has the absorption spectrum sensitive to the electrostatic changes due to the changes in charge occurring on the donor side of PSII.

In this study, two mutations close to Chl_{D1} have been designed and studied: the D1/T179H and the D1/T179V. In both mutants, the PSII remained fully active allowing us to get new insights on the Chl_{D1} involvement in PSII electron transfer. More generally, the data show that the presence of a histidine in a position that makes it a potential Chl_{D1} ligand or the presence of a valine, which is predicted to make Chl_{D1} almost symmetric to Chl_{D2}, did not greatly alter the PSII function despite the apparently lower energy level of $Chl_{D1}^{+}Pheo_{D1}^{-}$ radical pair in the T179H-PSII. In contrast, this decrease seems to favour the indirect charge recombination, which decreases the recombination route forming of the $^{3}Chl_{D1}$ triplet state,

making this mutant resistant to high light-induced photodamage *in vivo* and *in vitro*. It is worth comparing this photodamage-resistant mutant to strains isolated from extreme environments that seem naturally resistant to photoinhibition. This could represent a modification that could be engineered in strains for use in biotechnology. Similar mutants at the Chl_{D2} site could help in future studies to better understand the asymmetry in the environments of Ch_{D1} and Chl_{D2}.

Supplementary Material

Additional data are shown.

Acknowledgements

Collaboration between France and Japan was supported by JSPS-KAKENHI grant in Scientific Research on Innovative Areas "Innovations for Light-Energy Conversion (I^4LEC)" (JP17H06433). MS and TN were supported by JSPS-KAKENHI grant in Scientific Research on Innovative Areas JP17H06435 and JSPS KAKENHI grant JP17H03662, and MS was supported by a JSPS-KAKENHI grant JP17K07367. AB was supported by the French Infrastructure for Integrated Structural Biology (FRISBI) ANR-10-INBS-05. AWR was supported by BBSRC grant BB/R001383/1 and a grant from the Leverhulme Trust (PRG-2017-223).

References

1. M. Suga, F. Akita, K. Hirata, G. Ueno, H. Murakami, Y. Nakajima, T. Shimizu, K. Yamashita, M. Yamamoto, H. Ago, J.-R. Shen, Native structure of photosystem II at 1.95 angstrom resolution viewed by femtosecond X-ray pulses, Nature 517 (2015) 99–103.
2. Y. Umena, K. Kawakami, J–R. Shen, N. Kamiya, Crystal structure of oxygen–evolving Photosystem II at a resolution of 1.9 Å, Nature 473 (2011) 55–60.
3. B. Kok, B. Forbush, M. McGloin, Cooperation of charges in photosynthetic O_2 evolution–I. A linear four step mechanism, Photochem. Photobiol. 11 (1970) 457–475.
4. P. Joliot, B. Kok, Oxygen evolution in photosynthesis, in: Govindjee (Ed.), Bioenergetics of Photosynthesis, Academic Press, New York, 1975, pp. 387–412.
5. D.J. Nürnberg, J. Morton, S. Santabarbara, A. Telfer, P. Joliot, L.A. Antonaru, A.H. Ruban, T. Cardona, E. Krausz, A. Boussac, A. Fantuzzi, A.W. Rutherford, Photochemistry beyond the red-limit in the chlorophyll f-containing photosystems, Science 360 (2018) 1210–1213.
6. T. Cardona, A. Sedoud, N. Cox, A.W. Rutherford, Charge separation in Photosystem II: a comparative and evolutionary overview, Biochim. Biophys. Acta 1817 (2012) 26–43.
7. B.A. Diner, E. Schlodder, P.J. Nixon,| W.J. Coleman, F. Rappaport, J. Lavergne, W.F.J. Vermaas, D.A. Chisholm, Site-directed mutations at D1-His198 and D2-His197 of Photosystem II in *Synechocystis* PCC 6803: Sites of primary charge separation and cation and triplet stabilization, Biochemistry 24 (2001) 9265–9281.
8. E. Schlodder, T. Renger, G. Raszewski, W.J. Coleman, P.J. Nixon, R.O. Cohen, B.A. Diner, Site-directed mutations at D1-Thr179 of Photosystem II in *Synechocystis* sp. PCC 6803 modify the spectroscopic properties of the accessory chlorophyll in the D1-branch of the reaction center, Biochemistry 47 (2008) 3143–3154.
9. E. Schlodder, W.J. Coleman, P.J. Nixon, R.O. Cohen, T. Renger, B.A. Diner, Site-directed mutations at D1-His198 and D1-Thr179 of photosystem II in *Synechocystis* sp. PCC 6803: deciphering the spectral properties of the PSII reaction centre, Phil. Trans. R. Soc. B 363 (2008) 1197–1202.
10. A.R. Holzwarth, M.G. Müller, M. Reus, M. Nowaczyk, J. Sander, M. Rögner, Kinetics and mechanism of electron transfer in intact photosystem II and in the isolated reaction center: pheophytin is the primary electron acceptor, Proc. Natl Acad. Sci. USA 103 (2006) 6895–6900.

11. E. Romero, I.H.M. van Stokkum, V.I. Novoderezhkin, J.P. Dekker, R. van Grondelle, Two different charge separation pathways in Photosystem II, Biochemistry 49 (2010) 4300–4307.
12. H.-G. Duan, V.I. Prokhorenko, E. Wientjes, R. Croce, M. Thorwart, R.J. D. Miller, Primary charge separation in the Photosystem II reaction center revealed by a global analysis of the two-dimensional electronic spectra, Scientific Reports 7 (2017) 12347.
13. F.J.E. van Mieghem, K. Satoh, A.W. Rutherford, A chlorophyll tilted 30° relative to the membrane in the Photosystem II reaction centre, Biochim. Biophys. Acta, 1058 (1991) 379–385.
14. T. Noguchi, T. Tomo, C. Kato, Triplet formation on a monomeric chlorophyll in the photosystem II reaction center as studied by time-resolved infrared spectroscopy, Biochemistry 40 (2001) 2176–2185.
15. F. Müh, M. Plöckinger, T. Renger, Electrostatic asymmetry in the reaction center of Photosystem II, J. Phys. Chem. Lett. 8 (2017) 850–858.
16. G. Raszewski, B.A. Diner, E. Schlodder, T. Renger, Spectroscopic properties of reaction center pigments in photosystem II core complexes: Revision of the multimer model, Biophys. J. 95 (2008) 105–119.
17. K. Cser, I. Vass, Radiative and non–radiative charge recombination pathways in Photosystem II studied by thermoluminescence and chlorophyll fluorescence in the cyanobacterium *Synechocystis* 6803, Biochim. Biophys. Acta 1767 (2007) 233–243.
18. A.W. Rutherford, A. Krieger-Liszkay, Herbicide-induced oxidative stress in photosystem II, TIBS 26 (2001) 648–653.
19. F. Rappaport, M. Guergova-Kuras, P.J. Nixon, B.A. Diner, J. Lavergne, Kinetics and pathways of charge recombination in Photosystem II, Biochemistry 41 (2002) 8518–8527.
20. A.W. Rutherford, D.R. Paterson, J.E. Mullet, A light induced spin-polarized triplet detected by EPR in Photosystem II reaction centres, Biochim. Biophys. Acta 635 (1981) 205–214.
21. H. van Gorkom, Electron transfer in photosystem II, Photosynth. Res. 6 (1985) 97–112.
22. G.N. Johnson, A.W. Rutherford, A. Krieger, A change in the midpoint potential of the quinone Q_A in Photosystem II associated with photoactivation of oxygen evolution, Biochim. Biophys. Acta 1229 (1995) 202–207.

23. J. Buchta, M. Grabolle, H. Dau, Photosynthetic dioxygen formation studied by time-resolved delayed fluorescence measurements — Method, rationale, and results on the activation energy of dioxygen formation, Biochim. Biophys. Acta, 1767 (2007) 565–574.

24. M. Sugiura, Y. Osaki, F. Rappaport, A. Boussac, *Corrigendum* to "Influence of Histidine-198 of the D1 subunit on the properties of the primary electron donor, P_{680}, of Photosystem II in *Thermosynechococcus elongatus*, Biochim. Biophys. Acta 1857 (2016) 1943–1948.

25. M. Sugiura, Y. Inoue, Highly purified thermo-stable oxygen evolving Photosystem II core complex from the thermophilic cyanobacterium *Synechococcus elongatus* having His-tagged CP43, Plant Cell Physiol. 40 (1999) 1219–1231.

26. M. Sugiura, C. Azami, K. Koyama, A.W. Rutherford, F. Rappaport, A. Boussac, Modification of the pheophytin redox potential in *Thermosynechococcus elongatus* Photosystem II with PsbA3 as D1, Biochim. Biophys. Acta 1837 (2014) 139–148.

27. M. Ikeuchi, Y. Inoue, A new 4.8-kDa polypeptide intrinsic to the PS II reaction center, as revealed by modified SDS-PAGE with improved resolution of low-molecular-weight proteins, Plant Cell Physiol 29 (1988) 1233–1239.

28. A.U. Rehman, K. Cser, L. Sass, I. Vass, Characterization of singlet oxygen production and its involvement in photodamage of Photosystem II in the cyanobacterium Synechocystis PCC 6803 by histidine-mediated chemical trapping, Biochim. Biophys. Acta 1827 (2013) 689–698.

29. A. Telfer, S.M. Bishop, D. Phillips, J. Barber, Isolated photosynthetic reaction centre of Photosystem II as a sensitizer for the formation of singlet oxygen, J. Biol. Chem. 269 (1994) 13244−13253.

30. S. Styring, A.W. Rutherford, In the oxygen evolving complex of Photosystem II the S0 state is oxidized to the S1 state by D^+ (Signal II slow), Biochemistry 26 (1987) 2401–2405.

31. J.-M. Ducruet, Chlorophyll thermoluminescence of leaf discs: simple instruments and progress in signal interpretation open the way to new ecophysiological indicators, J. Exp. Bot. 54 (2003) 2419–2430.

32. J.-M. Ducruet, I. Vass, Thermoluminescence: experimental, Photosynth. Res. 201 (2009) 195–204.

33. D. Beal, F. Rappaport, P. Joliot, A new high–sensitivity 10–ns time–resolution spectrophotometric technique adapted to in vivo analysis of the photosynthetic apparatus, Rev. Sci. Instrum. 70 (1999) 202–207.

34. M. Sugiura, A. Boussac, T., Noguchi, F. Rappaport, Influence of Histidine-198 of the D1 subunit on the properties of the primary electron donor, P680, of Photosystem II in *Thermosynechococcus elongatus*, Biochim. Biophys. Acta 1777 (2008) 331−342.

35. T. Okubo, T. Tomo, M. Sugiura, T. Noguchi, Perturbation of the structure of P_{680} and the charge distribution on its radical cation in isolated reaction center complexes of photosystem II as revealed by Fourier transform infrared spectroscopy, Biochemistry 46 (2007) 4390–4397.

36. F. Rappaport, M. Blanchard-Desce and J. Lavergne, Kinetics of electron-transfer and electrochromic change during the redox transitions of the photosynthetic oxygen-evolving complex, Biochim. Biophys. Acta, 1184 (1994) 178–192.

37. J. Lavergne, Improved UV-visible spectra of the S-transitions in the photosynthetic oxygen-evolving system, Biochim. Biophys. Acta, 1060 (1991) 175–188.

38. D.H. Stewart, G.W. Brudvig, Cytochrome b559 of photosystem II, Biochim. Biophys. Acta 1367 (1998) 63–87.

39. J. Hanley, Y. Deligiannakis, A. Pascal, P. Faller, A.W. Rutherford, Carotenoid oxidation in photosystem II, Biochemistry 38 (1999) 8189–8195.

40. J.L. Hughes, A.W. Rutherford, M. Sugiura, E. Krausz, Quantum efficiency distributions of photo-induced side-pathway donor oxidation at cryogenic temperature in photosystem II, Photosynth. Res. 98 (2008) 199–206.

41. J.L. Hughes, N. Cox, A.W. Rutherford, E. Krausz, T.-L. Lai, A. Boussac, M. Sugiura, D1 protein variants in Photosystem II from *Thermosynechococcus elongatus* studied by low temperature optical spectroscopy, Biochim. Biophys. Acta 1797 (2010) 11–19.

42. E. Krausz, Selective and differential optical spectroscopies in photosynthesis, Photosynth. Res. 116 (2013) 411–426.

43. E. Krausz, N. Cox, S. Peterson Årsköld, Spectral characteristics of PS II reaction centres: as isolated preparations and when integral to PS II core complexes, Photosynth. Res. 98 (2008) 207–217.

44. A. Sedoud, PhD Thesis (2011): Transfert d'électrons dans le photosystème II, Paris-Sud University, Orsay, France.

45. D.L. Kirilovsky, A.G.P. Boussac, F.J.E. van Mieghem, J-M.R.C. Ducruet, P.R. Sétif, J. Yu, W.F.J. Vermaas, A.W. Rutherford, Oxygen-evolving Photosystem II preparation from wild type and Photosystem II mutants of *Synechocystis* Sp. PCC 6803, Biochemistry 31 (1992) 2099–2107.

46. M.Y. Okamura, K. Satoh, R.A. Isaacson, G. Feher, Evidence of the primary charge separation in the D-1/D-2 complex of photosystem II from spinach: EPR of the triplet state, in: J. Biggins (Ed.), Progress in Photosynthesis Research, vol. 1, Martinus Nijhoff, Dordrecht, 1981, pp. 379– 381.

47. F.J.E. van Mieghem, K. Brettel, B. Hillmann, A. Kamlowski, A.W. Rutherford, E. Schlodder, Charge recombination reactions in photosystem II: 1. Yields, recombination pathways, and kinetics of the primary pair, Biochemistry 34 (1995) 4798–4813.

48. F.J.E. van Mieghem, W. Nitschke, P. Mathis, A.W. Rutherford, The influence of the quinone-iron electron acceptor complex on the reation centre photochemistry of PS II, Biochim. Biophys. Acta 977 (1989) 207–214.

49. A.W. Rutherford, J.E. Mullet, Reaction centre triplet states in Photosystem I and Photosystem II Biochim. Biophys. Acta 635 (1981) 225-235.

50. P. Jordan, P. Fromme, H.T. Witt, O. Klukas, W. Saenger, N. Krauss, Three-dimensional structure of cyanobacterial photosystem I at 2.5 angstrom resolution, Nature 411 (2001) 909–917.

51. A.R. Corrie, J.H.A. Nugent, M.C.W. Evans, Identification of EPR signals from the states $Q_A^-Q_B^-$ and Q_B^- in Photosystem II from *Phormidium laminosum*, Biochim. Biophys. Acta 1057 (1991) 384–390.

52. C. Fufezan, C.-X. Zhang, A. Krieger-Liszkay, A.W. Rutherford, Secondary quinone in Photosystem II of *Thermosynechococcus elongatus*: Semiquinone-iron EPR signals and temperature dependence of electron transfer, Biochemistry 44 (2005) 12780–12789.

53. A. Sedoud, N. Cox, M. Sugiura, W. Lubitz, A. Boussac, A.W. Rutherford, The semiquinone-iron complex of Photosystem II: EPR signals assigned to the low field edge of the ground state doublet of $Q_A^{\bullet-}Fe^{2+}$ and $Q_B^{\bullet-}Fe^{2+}$, Biochemistry 50 (2011) 6012–6021.

54. E.G. Andrizhiyevskaya, A. Chojnicka, J.A. Bautista, B.A. Diner, R. van Grondelle, J.P. Dekker, Origin of the F685 and F695 fluorescence in Photosystem II, Photosynthesis Research 84 (2005) 173–180.

55. F. Rappaport, J. Lavergne, Proton release during successive oxidation steps of the photosynthetic water oxidation process: Stoichiometries and pH dependence, Biochemistry 30 (1991) 10004–10012.

56. A.Y. Mulkidjanian, D.A. Cherepanov, M. Haumann, W. Junge, Photosystem II of green plants: Topology of core pigments and redox cofactors as inferred from electrochromic difference spectra, Biochemistry 35 (1996) 3093–3107.

57. M. Sugiura, F. Rappaport, K. Brettel, T. Noguchi, A.W. Rutherford, A. Boussac, Site-directed mutagenesis of *Thermosynechococcus elongatus* photosystem II: the O_2 evolving enzyme lacking the redox active tyrosine D, Biochemistry 43 (2004) 13549–13563.

58. B.A. Diner, F. Rappaport, Structure, dynamics, and energetics of the primary photochemistry of photosystem II of oxygenic photosynthesis, Annu. Rev. Plant Biol. 53 (2002) 551–580.

59. A. Kamlowski, A. van der Est, D. Stehlik, The triplet state P-3(680) in Photosystem II studied with time-resolved EPR Mathis P (ed.) Photosynthesis: from Light to Biosphere, 1995, Vol I, pp 787-790, Kluwer Academic Publishers. Dordrecht.

60. M. Brecht, S. Skandary, J. Hellmich, C. Glöckner, A. Konrad, M. Hussels, A.J. Meixner, A. Zouni, E. Schlodder, Spectroscopic properties of photosystem II core complexes from *Thermosynechococcus elongatus* revealed by single-molecule experiments, Biochim. Biophys. Acta 1837 (2014) 773–781.

61. Y. Shibata, S. Nishi, K. Kawakami, J.-R. Shen, T. Renger, Photosystem II does not possess a simple excitation energy funnel: Time-resolved fluorescence spectroscopy meets theory, J. Am. Chem. Soc. 135 (2013) 6903−6914.

62. J. Hall, T. Renger, F. Müh, R. Picorel, E. Krausz, The lowest-energy chlorophyll of photosystem II is adjacent to the peripheral antenna: Emitting states of CP47 assigned via circularly polarized luminescence, Biochim. Biophys. Acta 1857 (2016) 1580–1593.

63. F. Rappaport, J. Lavergne, Thermoluminescence: theory, Photosynth. Res. 101 (2009) 205–216.

64. E. Romero, V.I. Novoderezhkin, R. van Grondelle, Quantum design of photosynthesis for bio-inspired solar-energy conversion, Nature 543 (2017) 355–365.

65. I. Vass, K. Cser, Janus-faced charge recombinations in photosystem II photoinhibition, Trends Biochem. Sci. 14 (2009) 200–205.

Legend of Figures

Figure 1:

Arrangement of cofactors for electron transfer in PSII including $Pheo_{D1}$ (A), structure of P_{D1} and P_{D2} with ligand amino acid residues (B), and structure around Chl_{D1} and Chl_{D2} (C). The figures were drawn with MacPyMOL with the A monomer in PDB 4UB6. D1/E130 in panel A was drawn by substituting E130 for Q130 in the PDB 4UB6 structure in which D1 is PsbA1.

Figure 2:

Construction and confirmation of the *psbA*$_3$ gene in the D1/T179H and the D1/T179V mutant cells. (A) Nucleotide sequence of *psbA*$_3$ and the amino acid sequences around PsbA3/Thr179 in the WT*3 strain and the D1/T179H and D1/T179V mutants. Positions of Thr179 is indicated with red letters. Numbers correspond to the position from the initial codon. Substituted nucleotides for T179H and T179V in the mutants are indicated in small letters. For making and selection of mutants, the *Msc* I and *Bsa*H I restriction sites (letters in italic) were created in T179H and T179V, respectively, in the same time. (B) Physical map around *psbA*$_3$, and theoretical length of amplified DNA by PCR using *Forward (Fw)* and *Reverse (Rv)* primers. The created *Msc* I (shown as *Msc* I*) and *Bsa*H I (shown as *Bsa*H I*) sites for the T179H and T179V mutants, respectively, are at position +533. The DNA fragments of 554 bp was digested with *Msc* I into 216 bp and 338 bp (T179H), and digested with *Bsa*H I into 215 bp and 339 bp (T179V) (C). Agarose gel (2%) electrophoresis of PCR products using the *Fw* and *Rv* primers (lanes 2 and 4) and the DNA fragments of the products after digestion with *Msc* I (lanes 3) and with *Bsa*H I (lane 5). Lane 1, 100 bp DNA ladder markers (Nacalai, Japan); lanes 2 and 3, T179H strain; lanes 4 and 5, T179V strain.

Figure 3:

Sequence of the amplitude of the absorption changes at 292 nm using a series of saturating flashes (spaced 300 ms apart) and given to WT*3-PSII (black trace), T179H-PSII (red trace) and T179V-PSII (blue trace). The samples ([Chl] = 25 μg/ml) were dark-adapted for 1 h at room temperature before the addition of 100 μM PPBQ dissolved in DMSO. The measurements were done 100 ms after each flash.

Figure 4:

Light-*minus*-dark difference absorption spectra recorded at 77 K. After the recording of the spectrum on the dark-adapted samples illumination at 77 K was given before the recording of the light spectrum on WT*3-PSII (black spectrum), T179H-PSII (red spectrum), T179V-PSII (blue spectrum) and H198Q-PSII (green spectrum in Panel B). Panel A shows the spectral region including the C-550 band-shift and the α-band of Cytb_{559}. Panel B shows the spectral region including the reaction Q_Y electrochromisms. The light-*minus*-dark spectrum in H198Q-PSII was multiplied by a factor 1.3 to normalize its amplitude to the same amount of Q_A^- as in the 3 other samples. Indeed, the amplitude of the C-550 band-shift was 1.3 times smaller in this sample.

Figure 5:

Flash-induced absorption changes measured in WT*3-PSII (black trace), T179H-PSII (red trace) and T179V-PSII (blue trace) 5 ns after the first flash given on dark-adapted PSII. Upon dark-adaptation for 1 h at room temperature, 100 μM PPBQ (dissolved in DMSO) was added to the samples with [Chl] = 25 μg mL^{-1}.

Figure 6:

Triplet EPR signals in WT*3-PSII (black trace), T179H-PSII (red trace) and T179V-PSII (blue trace). The samples were pretreated with 40 mM dithionite and illumination at room temperature followed by dark adaptation before freezing [47,48]. Panel A shows the full spectra and Panels B and C show the external lines with an expended magnetic field scale in WT*3-PSII (black trace) and T179H-PSII (red trace). The spectra are light-*minus*-dark-spectra recorded at 4.2 K under illumination and in the dark after the illumination. Instrument settings: modulation amplitude, 25 G; microwave power, 63 μW; microwave frequency, 9.4 GHz; modulation frequency, 100 kHz. The saturated radical signal centered at ~ 3385 gauss has been deleted.

Figure 7:

Thermoluminescence glow curves from $S_2Q_A^-$/DCMU charge recombination measured after one flash given at 0°C in WT*3-PSII (black trace), T179H-PSII (red trace) and T179V-PSII (blue trace). The samples were previously dark-adapted at room temperature for 1 h before the addition of DCMU and being loaded into the cuvette and illuminated. The heating rate was 0.7°C/s.

Figure 8:

EPR spectra recorded in WT*3-PSII (Panel A), T179H-PSII (Panel B) and T179V-PSII (Panel C). Spectra were recorded either after white light illumination at 198 K (dark spectra) or after a further dark period of 5 minutes at room temperature following the illumination at 198 K (red spectra). [Chl] = 1.1 mg·mL^{-1}. Instrument settings: Temperature, 8.6 K; modulation amplitude, 25 G; microwave power, 20 mW; microwave frequency, 9.4 GHz; modulation frequency, 100 kHz. The saturated signal centered at ~ 3385 gauss originated from $Tyr_D^{\bullet}$.

Figure 9:

Panel A: O_2 consumption measured under illumination at 20,000 µmol photons m^{-2} s^{-1} in the presence of 10 mM L-histidine and 25 µM DCMU with WT*3-PSII (black trace), T179H-PSII (red trace) and T179V-PSII (blue trace). The arrow indicates the starting point of light irradiation. The data are the average of 3 independent measurements. Panel B: difference spectra measured at room temperature in WT*3-PSII (black spectrum), T179H-PSII (red spectrum) and T179V-PSII (blue spectrum) after-*minus*-before high light illumination given at 45°C with a light intensity of ≈ 500 µmol photons m^{-2} s^{-1}. Panel C: difference spectra between 650 and 700 nm measured at 77 K in WT*3-PSII (black spectrum), T179H-PSII (red spectrum) and T179V-PSII (blue spectrum) after-*minus*-before high light illumination. The PSII samples were arbitrarily normalized to the same amplitude at 673 nm. Panel D: Difference spectra "after-*minus*-before" high light illumination measured at room temperature in WT*3-PSII (black trace), T179H-PSII (red trace) and T179V-PSII (blue trace). The spectra were arbitrarily scaled to the same amplitude.

Figure 10:

Fluorescence spectra recorded at 77 K in WT*3-PSII (black trace), T179H-PSII (red trace) and T179V-PSII (blue trace). The wavelength of the light for the fluorescence excitation was 440 nm.

Figure 11:

Panel A: Flash-induced absorption changes measured 100 ms after each of the first 6 flashes given to dark-adapted WT*3-PSII. Panel B: Sequence of the amplitude of the absorption changes 440 nm-*minus*-428 nm measured as in Panel A in WT*3-PSII (black trace), T179H-

PSII (red trace) and T179V-PSII (blue trace). Panel C: Flash-induced absorption changes measured 100 ms after the 3rd flash given to WT*3-PSII (black trace), T179H-PSII (red trace) and T179V-PSII (blue trace). Upon dark-adaptation for 1 h at room temperature, 100 μM PPBQ (dissolved in DMSO) was added to the samples with [Chl] = 25 μg mL^{-1}.

Figure 12:

A simplified scheme of the energetics (on a standard free energy scale) and recombination pathways in the D1/T179H-PSII compared to the wild type that could explain the main phenomena reported in the present work. The energy levels of all states are taken to be the same in both variant forms except for a decrease in the energy level of the primary radical pair, [$Chl_{D1}^{+}Pheo_{D1}^{-}$], in the mutant (in red). The energy gaps are not to scale. The energy scale is broken as indicated by the line breaks. Only the cofactors involved in the primary reactions are shown, the other cofactors (Tyr_Z, P_{D2}, Mn_4O_5Ca, Q_B, the side-path electron donors) are relevant to the experiments but not to the mechanism illustrated. For the sake of clarity the spin-state of the radical pairs are not shown. The triplet form of the primary radical pair, ^{3}[$Chl_{D1}^{+}Pheo_{D1}^{-}$], can recombine to form the $^3Chl_{D1}$ triplet state, while the singlet form of the same radical pair can recombine to form the excited singlet state or the ground state. At room temperature the excited singlet state is expected to be shared over all the chlorophylls in PSII and any of these can be radiative (not shown). The small change in the color of Chl_{D1} represents a small decrease in the energy level of $^*Chl_{D1}$ but this is taken to be negligible in the scheme. The decrease in the energy level of the primary radical pair in the mutant results in *i*) a decrease in the radiative route (indicated by the thinner green arrows back to the excited state), *ii*) less energy required to reform the primary radical pair (a smaller energy gap for the back-reaction from the secondary radical pair [$P_{D1}^{+}Pheo_{D1}^{-}$]) favoring formation of the primary radical pair (thicker green line), *iii*) lower yield of triplet due to less efficient formation from the primary radical pair (as indicated by the thinner orange arrow) due to less driving force, as illustrated and/or with a possible more favorable direct recombination (red k_i^2 *vs* black k_i^2) from the radical pair (as expected considering this reaction is likely to be in the inverted Marcus region [65]. The situation shown is not a unique solution but it has the advantage of remaining within current models and relying on a single phenomenon, a single redox change (a decrease in the potential of Chl_{D1}). It provides a simple working model that can be tested by future experimentation on these and related mutants.

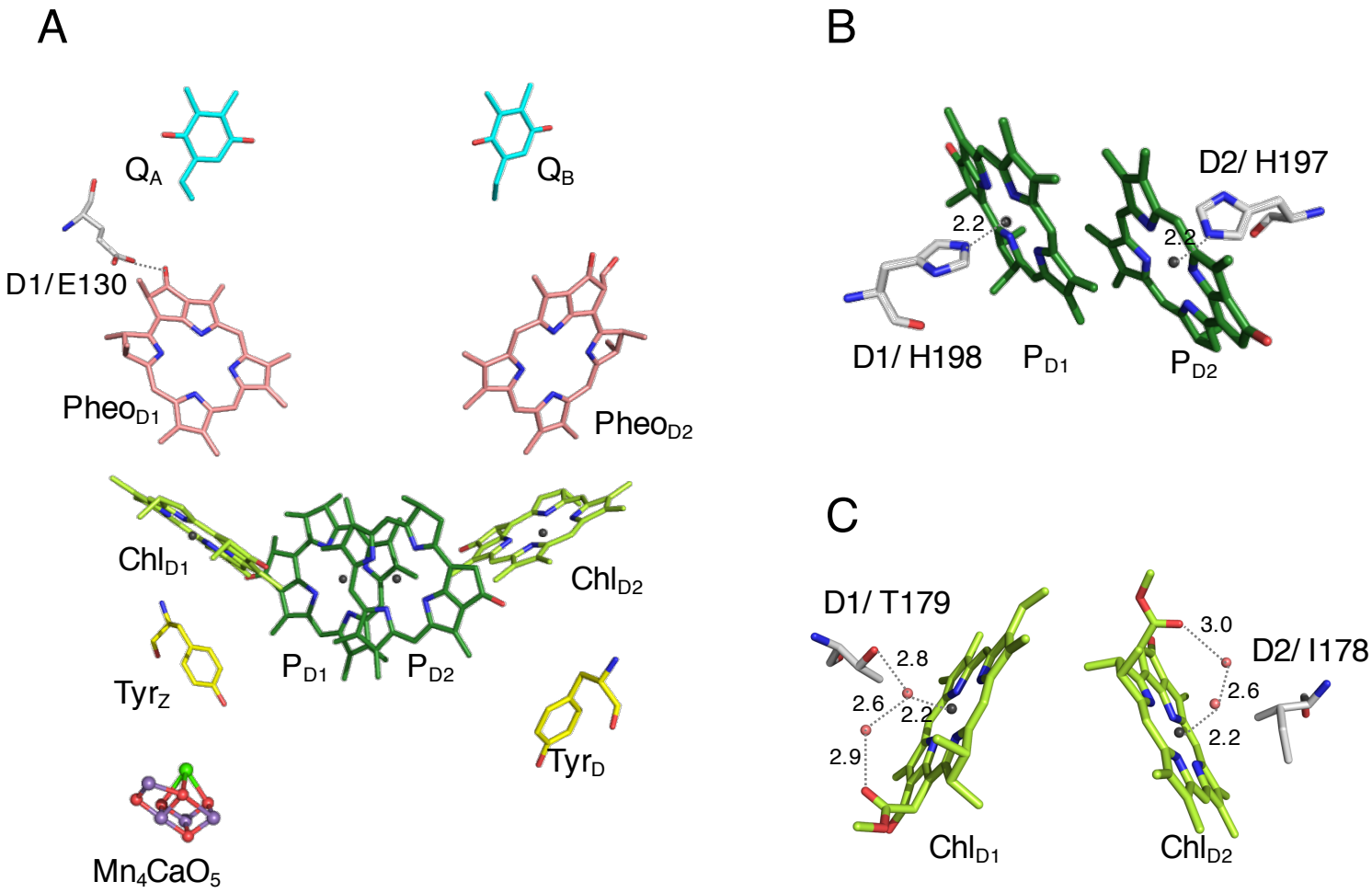
A
Q_A
Q_B
D1/E130
$Pheo_{D1}$
$Pheo_{D2}$
Chl_{D1}
Chl_{D2}
P_{D1}
P_{D2}
Tyr_Z
Tyr_D
Mn_4CaO_5
B
D2/ H197
2.2
2.2
D1/ H198
P_{D1}
P_{D2}
C
D1/ T179
2.8
2.6
2.2
2.9
Chl_{D1}
3.0
D2/ I178
2.6
2.2
Chl_{D2}

Figure 1

A

wild type *psbA*$_3$

```
          520        530        540        550
•••••ATGCCCCTCGGTATCTCTGGTACCTTCAACTTCATGCTTGTGTTC•••••
      M  P  L  G  I  S  G  T  F  N  F  M  L  V  F
```

Msc I*

```
T179H •••••CTCGGTATCTCTGGCcaCTTCAACTTCATG•••••
            L  G  I  S  G  H  F  N  F  M
```

*Bsa*H I*

```
T179V •••••CTCGGTATCTCTGGCgtCTTCAACTTCATG•••••
            L  G  I  S  G  V  F  N  F  M
```

B

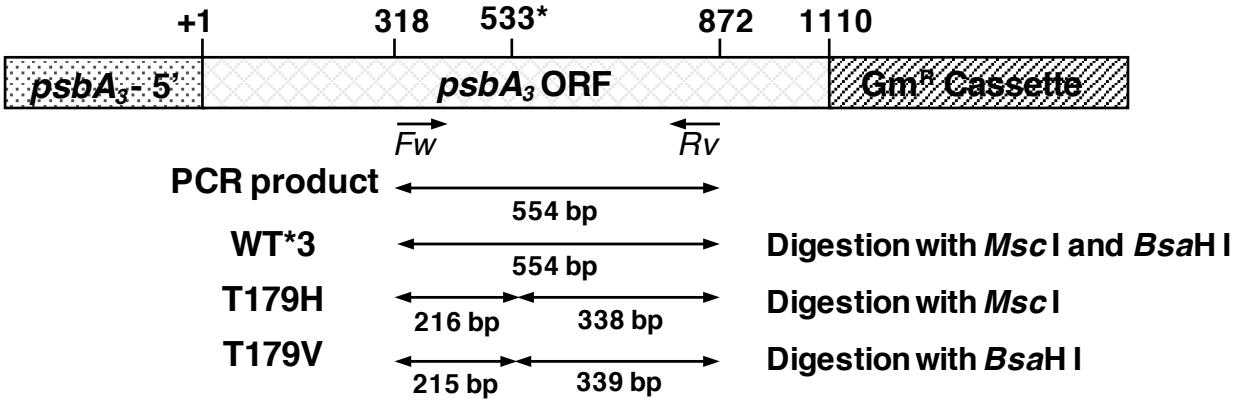

C

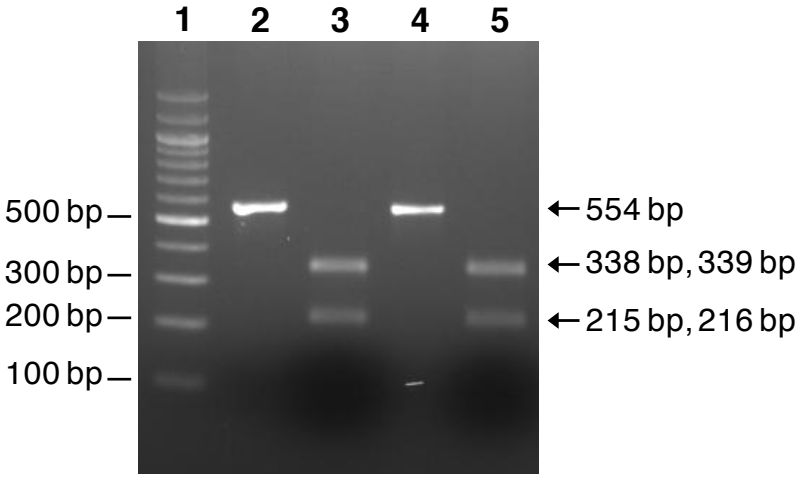

Figure 2

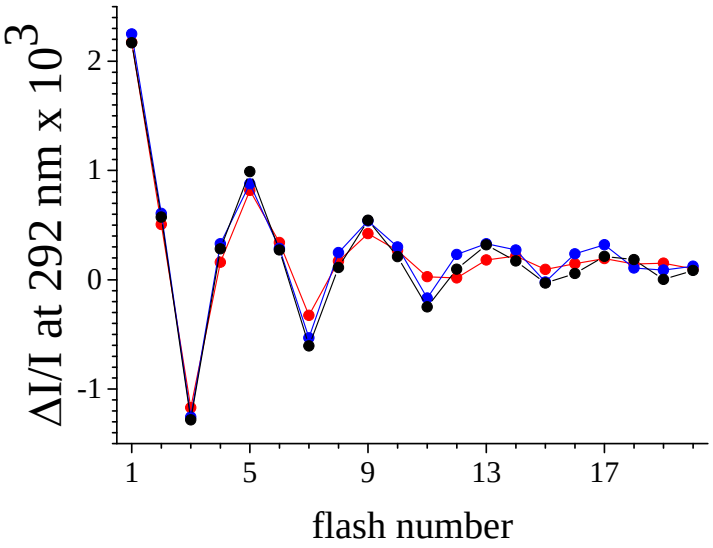

Figure 3

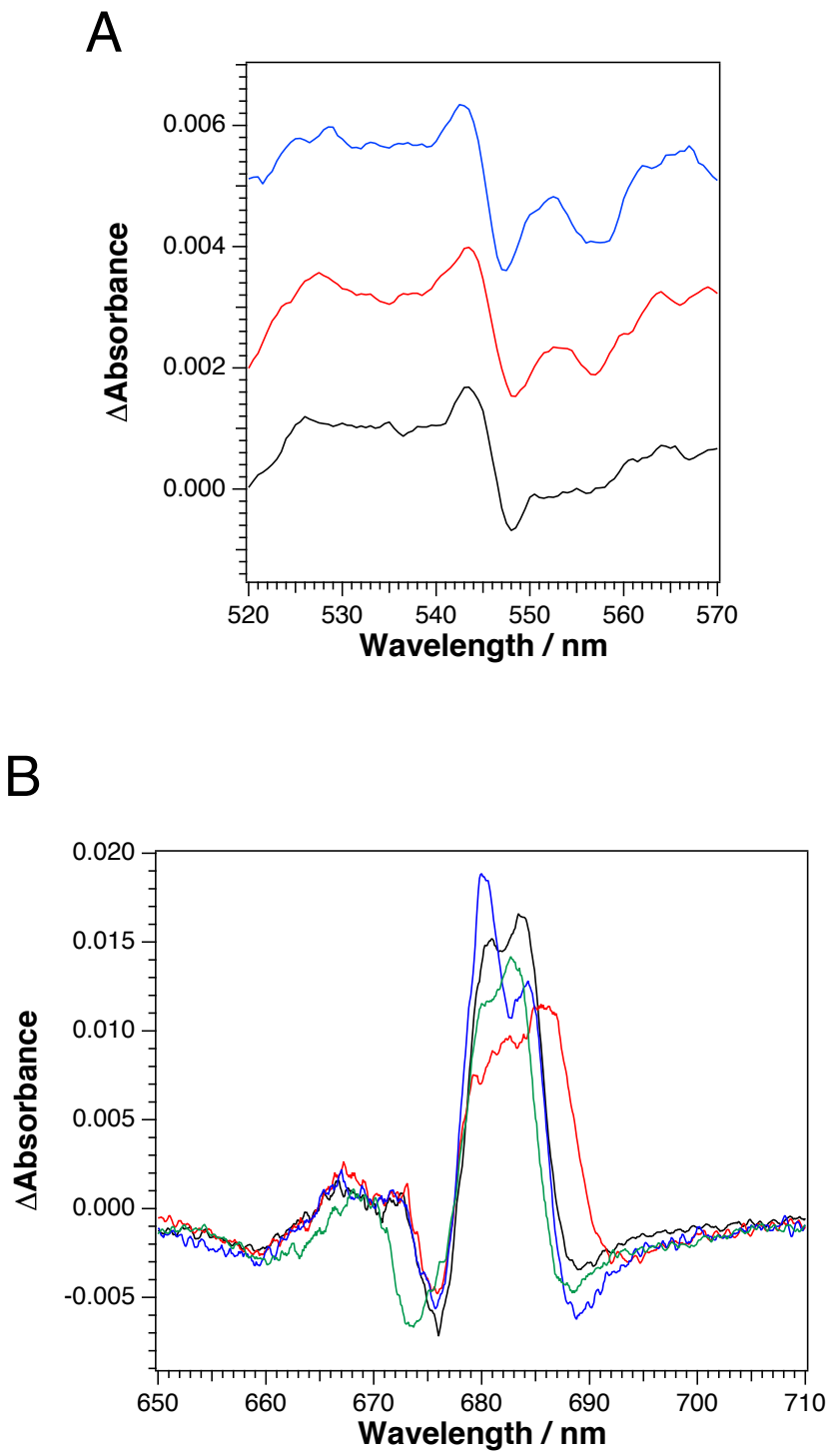
A
0.006
0.004
0.002
0.000
ΔAbsorbance
520
530
540
550
560
570
Wavelength / nm
B
0.020
0.015
0.010
0.005
0.000
-0.005
ΔAbsorbance
650
660
670
680
690
700
710
Wavelength / nm

Figure 4

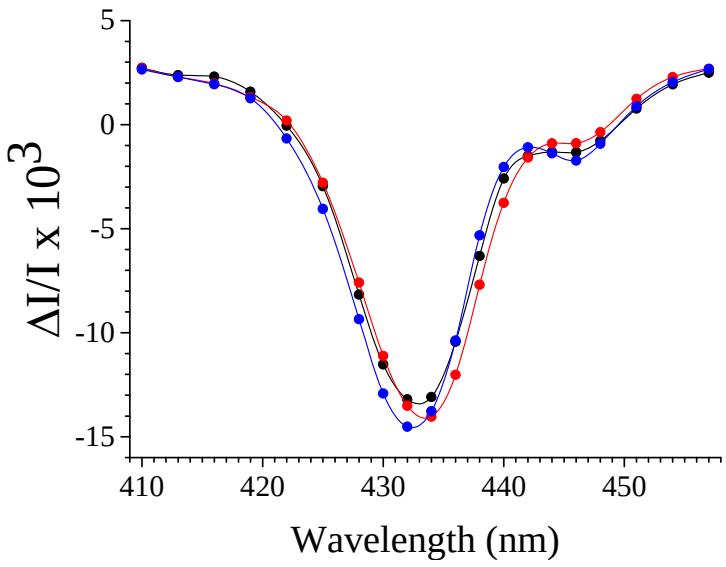

Figure 5

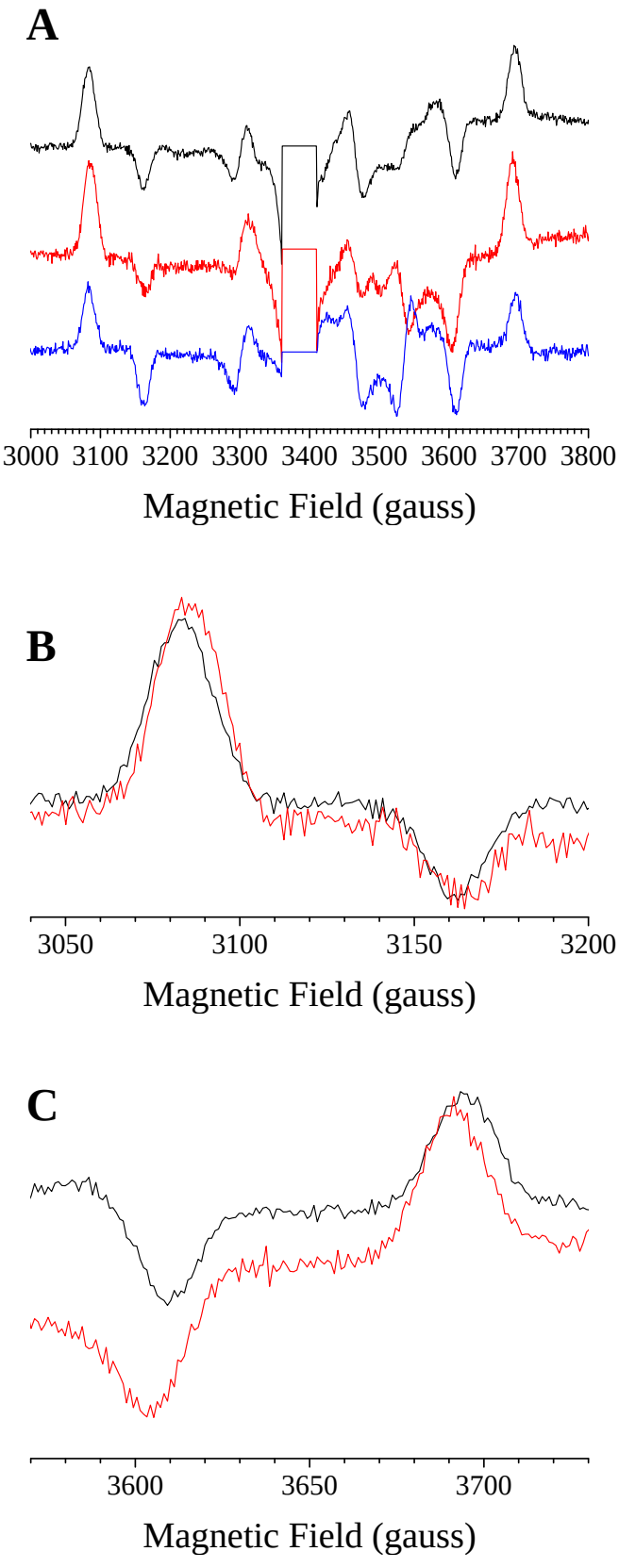
A
3000 3100 3200 3300 3400 3500 3600 3700 3800
Magnetic Field (gauss)
B
3050 3100 3150 3200
Magnetic Field (gauss)
C
3600 3650 3700
Magnetic Field (gauss)

Figure 6

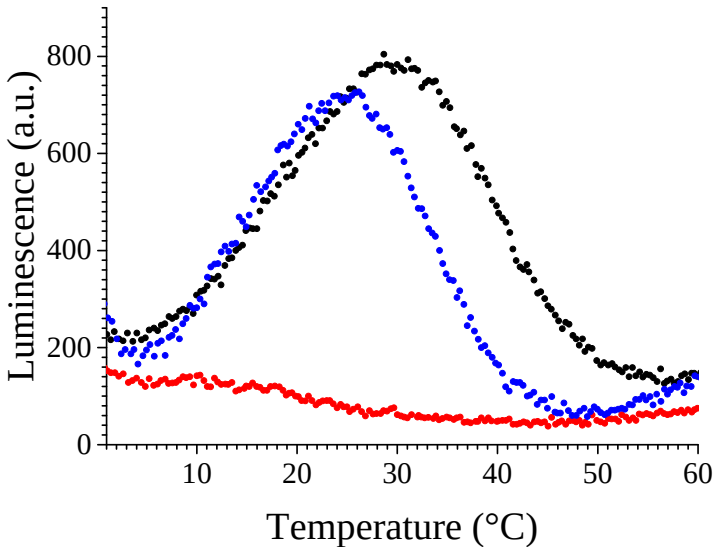
Luminescence (a.u.)
800
600
400
200
0
10
20
30
40
50
60
Temperature (°C)

Figure 7

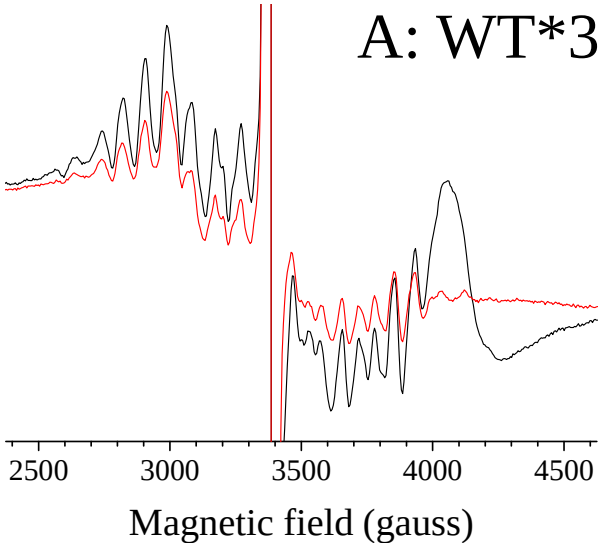
A: WT*3
2500
3000
3500
4000
4500
Magnetic field (gauss)

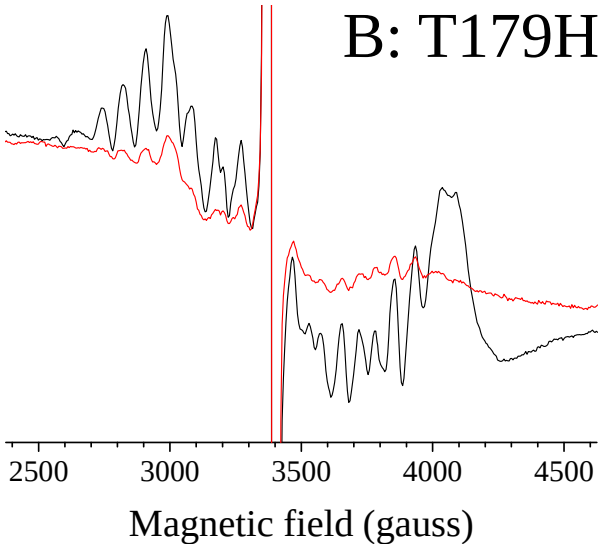
B: T179H
2500
3000
3500
4000
4500
Magnetic field (gauss)

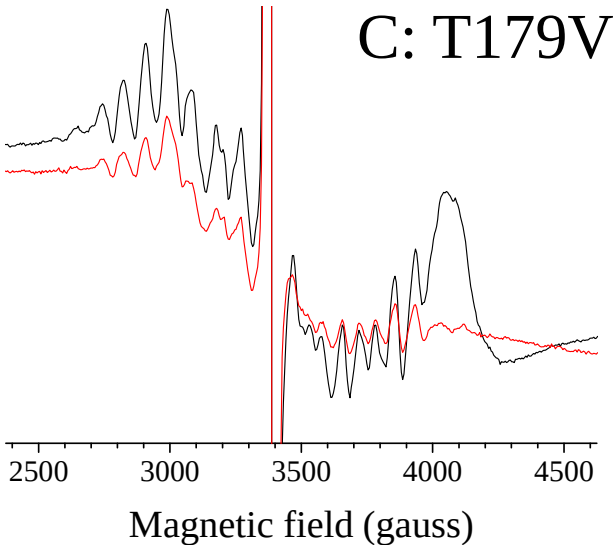
C: T179V
2500
3000
3500
4000
4500
Magnetic field (gauss)

Figure 8

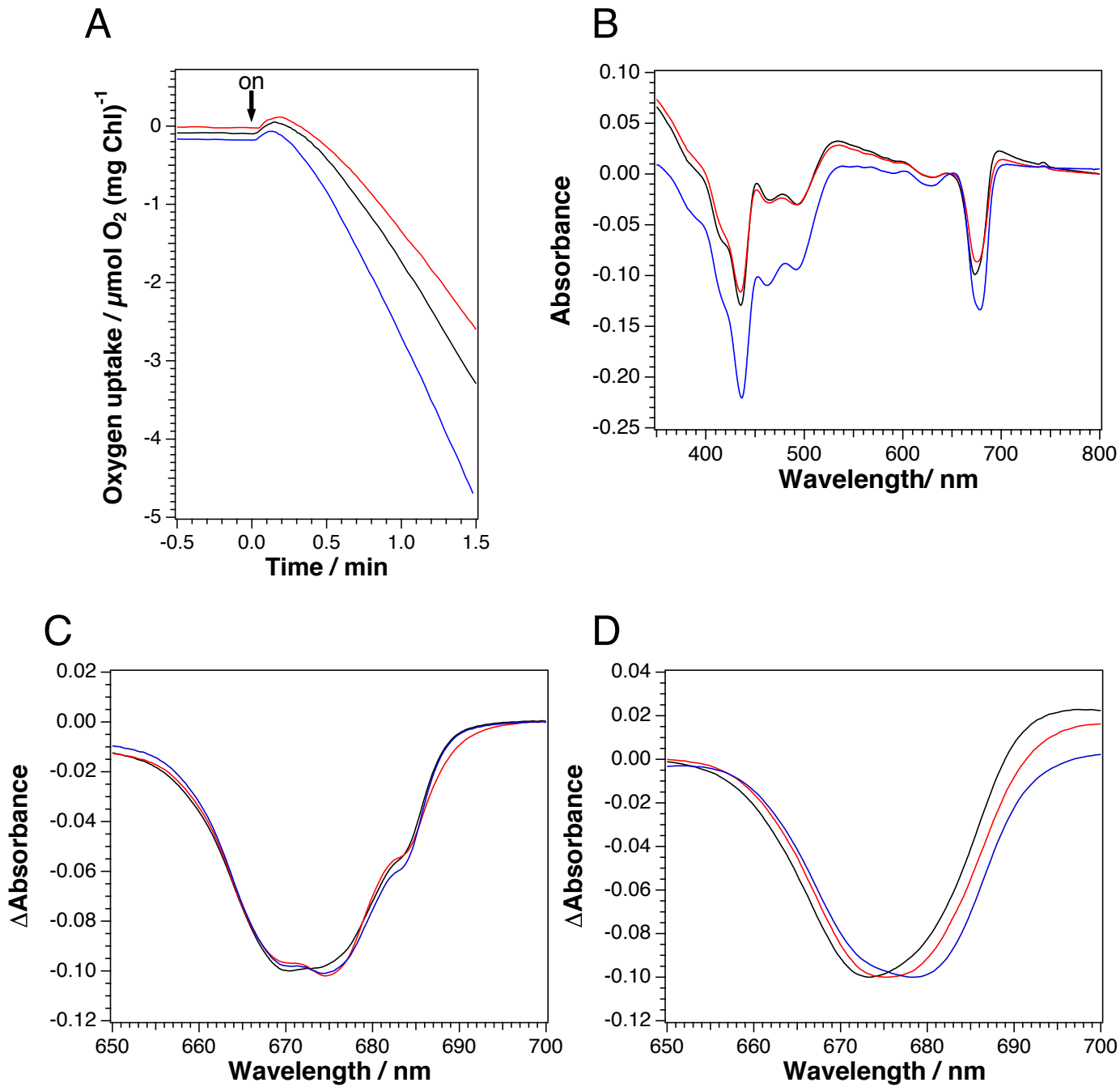
A
on
Oxygen uptake / µmol O2 (mg Chl)-1
0
-1
-2
-3
-4
-5
-0.5
0.0
0.5
1.0
1.5
Time / min
B
Absorbance
0.10
0.05
0.00
-0.05
-0.10
-0.15
-0.20
-0.25
400
500
600
700
800
Wavelength/ nm
C
ΔAbsorbance
0.02
0.00
-0.02
-0.04
-0.06
-0.08
-0.10
-0.12
650
660
670
680
690
700
Wavelength / nm
D
ΔAbsorbance
0.04
0.02
0.00
-0.02
-0.04
-0.06
-0.08
-0.10
-0.12
650
660
670
680
690
700
Wavelength / nm

Figure 9

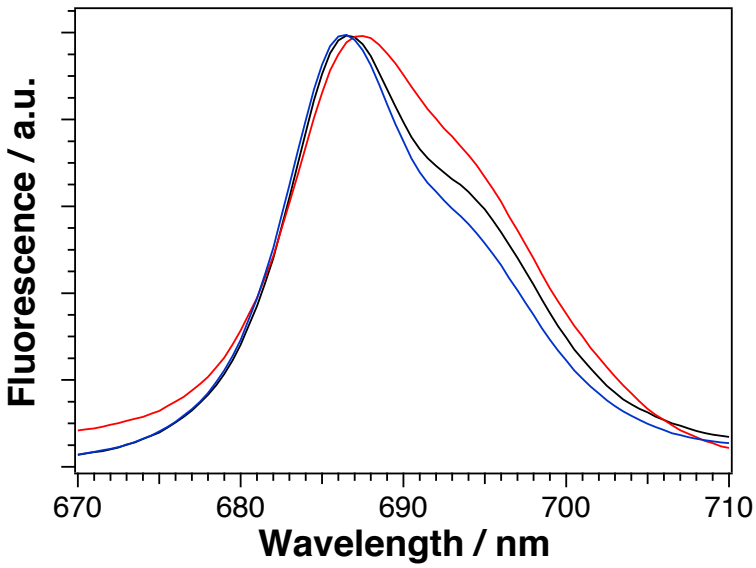

Figure 10

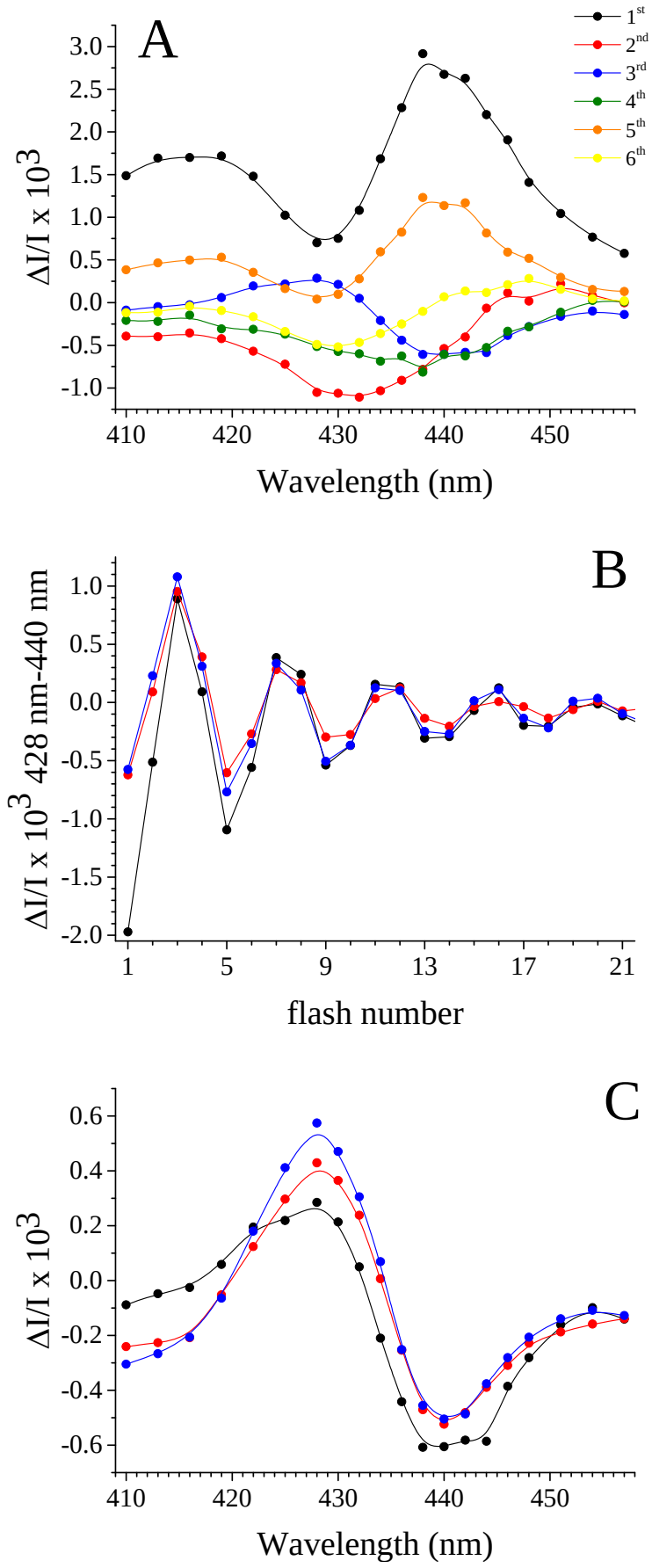
A
1st
2nd
3rd
4th
5th
6th
ΔI/I x 10^3
Wavelength (nm)
B
ΔI/I x 10^3 428 nm-440 nm
flash number
C
ΔI/I x 10^3
Wavelength (nm)

Figure 11

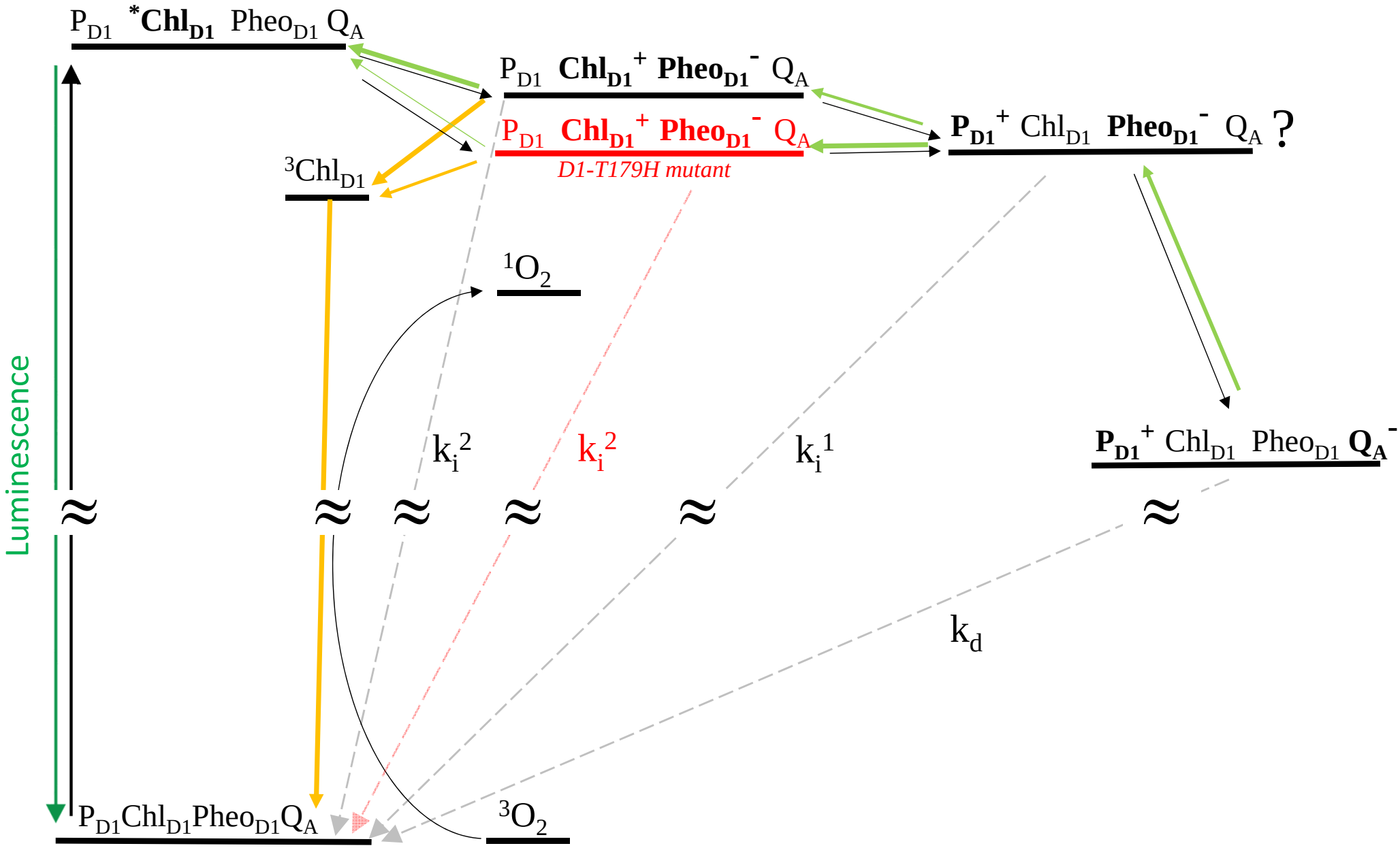
P_D1 *Chl_D1 Pheo_D1 Q_A
P_D1 Chl_D1+ Pheo_D1- Q_A
P_D1 Chl_D1+ Pheo_D1- Q_A
D1-T179H mutant
P_D1+ Chl_D1 Pheo_D1- Q_A ?
3Chl_D1
1O_2
Luminescence
k_i2
k_i2
k_i1
P_D1+ Chl_D1 Pheo_D1 Q_A-
k_d
P_D1Chl_D1Pheo_D1Q_A
3O_2

Figure 12